Multivalent Dynamic Colocalization of Avian Influenza Polymerase and Nucleoprotein by Intrinsically Disordered ANP32A Reveals the Molecular Basis of Human Adaptation

Aldo Camacho-Zarco, Lefan Yu, Tim Krischuns, Selin Dedeoglu, Damien Maurin, Guillaume Bouvignies, Thibaut Crépin, Rob Ruigrok, Stephan Cusack, Nadia Naffakh, et al.

JACS
JOURNAL OF THE AMERICAN CHEMICAL SOCIETY
pubs.acs.org/JACS

Article

Multivalent Dynamic Colocalization of Avian Influenza Polymerase and Nucleoprotein by Intrinsically Disordered ANP32A Reveals the Molecular Basis of Human Adaptation

Aldo R. Camacho-Zarco,[¶] Lefan Yu,[¶] Tim Krischuns, Selin Dedeoglu, Damien Maurin, Guillaume Bouvignies, Thibaut Crépin, Rob W. H. Ruigrok, Stephan Cusack, Nadia Naffakh, and Martin Blackledge*

Cite This: J. Am. Chem. Soc. 2023, 145, 20985−21001

ABSTRACT: Adaptation of avian influenza RNA polymerase (FluPol) to human cells requires mutations on the 627-NLS domains of the PB2 subunit. The E627K adaptive mutation compensates a 33-amino-acid deletion in the acidic intrinsically disordered domain of the host transcription regulator ANP32A, a deletion that restricts FluPol activity in mammalian cells. The function of ANP32A in the replication transcription complex and in particular its role in host restriction remains poorly understood. Here we characterize ternary complexes formed between ANP32A, FluPol, and the viral nucleoprotein, NP, supporting the putative role of ANP32A in shuttling NP to the replicase complex. We demonstrate that while FluPol and NP can simultaneously bind distinct linear motifs on avian ANP32A, the deletion in the shorter human ANP32A blocks this mode of colocalization. NMR reveals that NP and human-adapted FluPol, containing the E627 K mutation, simultaneously bind the identical extended linear motif on human ANP32A in an electrostatically driven, highly dynamic and multivalent ternary complex. This study reveals a probable molecular mechanism underlying host adaptation, whereby E627K, which enhances the basic surface of the 627 domain, is selected to confer the necessary multivalent properties to allow ANP32A to colocalize NP and FluPol in human cells.

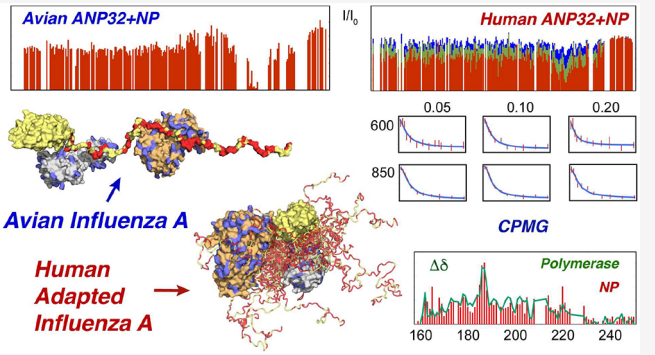

INTRODUCTION

Influenza A viruses (IAV) infect both mammals and aquatic birds, their natural hosts. Some highly pathogenic zoonotic avian strains, such as H5N1, can adapt to infect humans with high mortality, posing a serious pandemic threat.[1,2] Genome replication in IAV is performed by the RNA-dependent RNA polymerase (FluPol), a heterotrimer, comprising three proteins, PA, PB1, and PB2, that assemble in the nucleus of the infected cell.[3] The viral genome is made up of eight single-stranded, negative-sense RNA segments, each encapsidated by multiple viral nucleoproteins (NPs), and associated with FluPol to form ribonucleoprotein complexes (vRNPs). Replication requires two steps, first forming a complementary (cRNA), positive sense copy of the genome, that is then used as a template to synthesize the viral RNA (vRNA) replicate. This process has been suggested to involve two FluPol heterotrimers, one intrinsic to the vRNP, responsible for synthesis, and a second that controls encapsidation.[4−7]

Among other adaptations, mutations on the surface of FluPol are necessary in order to efficiently replicate in human cells. Adaptive mutations of avian IAV FluPol that are necessary for human infection are located to the C-terminal "627" and "NLS" domains of PB2.[8,9] This region of PB2 is highly dynamic,[8,10] with "open" and "closed" forms that interchange in a conformational equilibrium (Figure 1),[11] a dynamic character that is retained in the assembled polymerase, suggesting a role in the viral replication cycle.[12,13] Perhaps most remarkably, mutation of position 627 from E to K in avian PB2 rescues polymerase activity and viral replication in mammalian cells, spurring intense investigation into the molecular origin of this phenomenon.[14−17] Barclay and coworkers identified members of the ANP32 family, host transcription factors comprising a Leucine-rich region (LRR), followed by a highly acidic intrinsically disordered domain (IDD),[18,19] as responsible for this adaptation.[20] The IDD

Received: July 1, 2023
Published: September 14, 2023

https://doi.org/10.1021/jacs.3c06965
J. Am. Chem. Soc. 2023, 145, 20985−21001

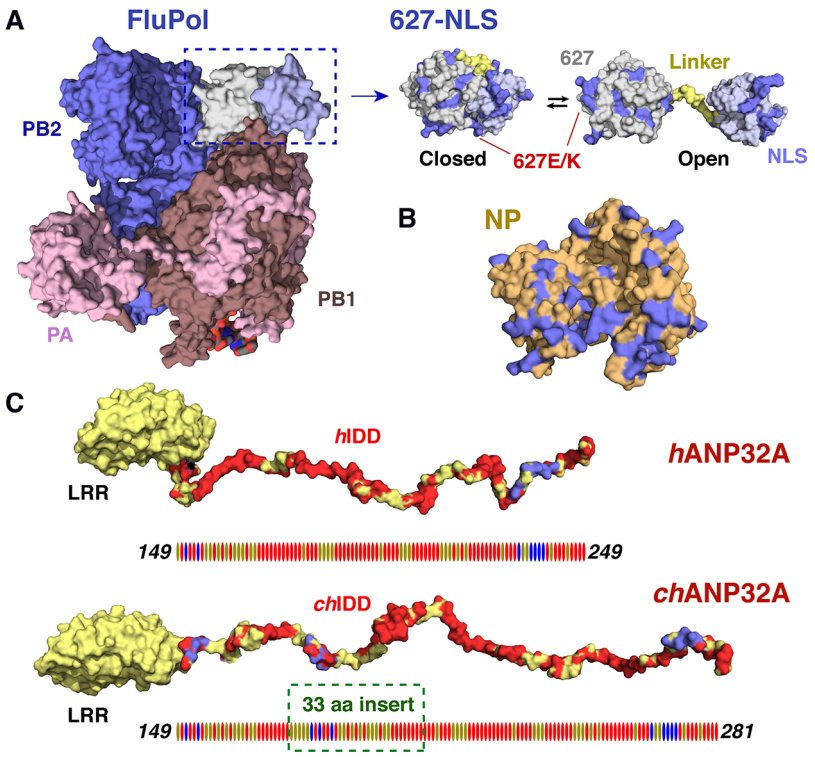

Figure 1. Viral and host proteins involved in influenza A replication. (A) Influenza polymerase (FluPol, vRNA bound form shown here, pdb code 4wsb[63]) comprises three subunits: PA, PB1, and PB2. Mutations in the 627 and NLS domains of PB2 (boxed) are crucial for adaptation from birds to mammals, in particular the E627K mutation is thought to compensate differences in the length of the host factor ANP32A.[20] These two domains have been shown to populate both open and closed conformations that are in dynamic equilibrium.[11] Positively charged residues of 627-NLS are shown in blue. (B) The viral nucleoprotein (NP) is a basic protein (monomeric mutant pdb code 3zdp shown here,[48] positively charged residues in blue) that binds the newly synthesized nascent RNA, and has also been shown to interact with ANP32A.[47] In this study, we investigate putative ternary complexes between the two viral proteins mediated by the avian and human host factors. (C) The host factor ANP32A comprises a folded leucine rich region (LRR) and a highly acidic intrinsically disordered domain (IDD), that is 33 amino acids longer in chicken (and most other birds) than in humans (and other mammals). The interaction between human ANP32A and human adapted 627(K)-NLS involves a multivalent interaction between the negatively charged IDD and the positively charged surface of 627(K).[32] This multivalency is not observed in the case of chicken ANP32A and avian adapted 627(E)-NLS.

exhibits an important difference across species, with a 33 amino acid deletion in human ANP32A (*hu*ANP32A) compared to avian ANP32A, consisting of an avian-unique hydrophobic hexapeptide followed by a repeat sequence of the preceding 27 amino acids (149−176) (Figure 1). This avian-specific insertion alone was also shown to be sufficient to rescue avian-adapted H5N1 FluPol activity in mammalian cells, suggesting a mechanistic correlation between the E627K mutation and differences in the IDDs of host ANP32A.[21−31] Numerous studies have further identified the interaction of ANP32A, and the related ANP32B,[27−29] with FluPol as critical to replication.[23,25,26] We recently described the complexes formed between the 627-NLS domains of human- and avian-adapted FluPol (627(K)-NLS and 627(E)-NLS, respectively) with *hu*ANP32A and chicken ANP32A (*ch*ANP32A),[32,33] revealing that while the unique hexapeptide present in the avian IDD binds to 627(E)-NLS, the interaction is very different in human-adapted complex, where the E627K mutation completes a basic surface on the 627 domain,[9] thereby allowing multivalent, transient interactions with a 50-amino acid stretch of the predominantly acidic IDD to stabilize the highly dynamic *hu*ANP32A:627(K)-NLS complex.

ANP32A is thought to be required primarily for viral genome replication,[21,26,34,35] and it has recently been shown that 627E restricts vRNA but not cRNA synthesis in mammalian cells.[36] Fodor and co-workers recently determined the structures of the complexes of *hu*ANP32A and *ch*ANP32A with FluPol from influenza C, bound to a 47-nucleotide vRNA.[37] FluPol adopts an asymmetric dimeric form, comprising an active replicase, and a second FluPol, apparently acting as an encapsidase. In complex, the folded LRR domain of ANP32A bridges the two 627 domains.

Despite these advances, the role of ANP32A in influenza replication is not understood at the molecular level. Many single-stranded, negative-sense RNA viruses express a phosphoprotein (P), that chaperones the nucleoprotein (N),[38−41] protecting against nonspecific binding to cellular RNA prior to encapsidation, and controlling nucleoprotein concentration in the vicinity of the viral polymerase, for example, by forming membraneless organelles.[42−46] Influenza does not express such a protein, which raises the question of whether host ANP32A can compensate the absence of such a viral adaptor protein by performing similar functions. Recent biochemical, pull-down, and mutagenesis studies have indeed demonstrated interaction of the disordered domain of ANP32A with NP, implicating the RNA-binding grooves on the surface of NP and the N-terminal half of the IDD of ANP32A as likely interaction sites.[47]

Here we describe the interaction of influenza NP with avian and human ANP32A at atomic resolution using NMR spectroscopy. We discover that the NP binding sites of ANP32A are located in the IDDs, and shifted by 33 amino

https://doi.org/10.1021/jacs.3c06965
J. Am. Chem. Soc. 2023, 145, 20985−21001

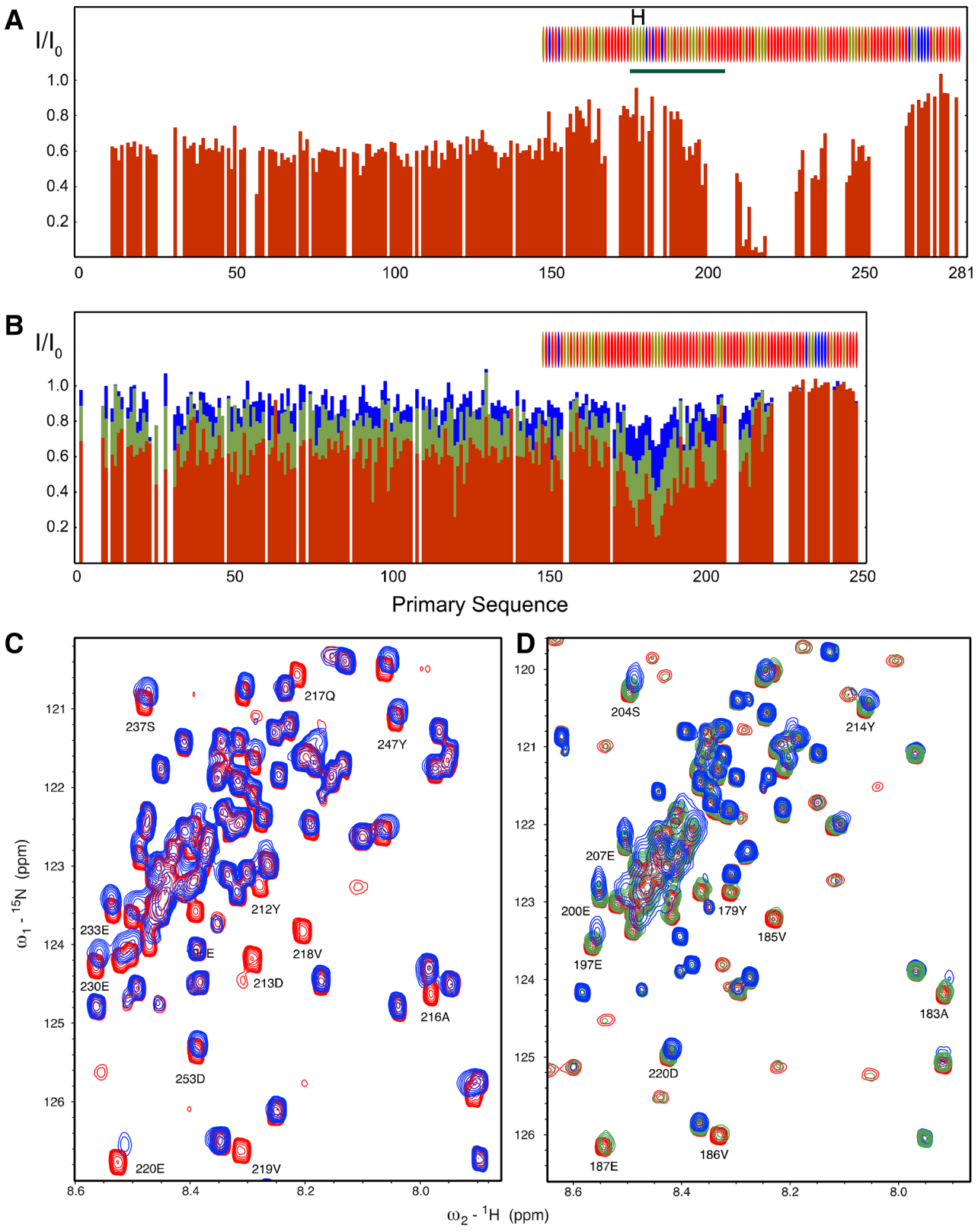

Figure 2. NP binds *ch* and *hu*ANP32A in the presence of increasing NP. (A) Intensities ratios of free and bound *ch*ANP32A. NP was added to 200 μM of ^{15}N *ch*ANP32A at a 1:0.5 ratio (BEST-TROSY at 700 MHz). Bars show intensity ratio with respect to the free spectrum. The amino acid distribution of the IDD of *ch*ANP32A and *hu*ANP32A is shown above plots A and B, respectively. Red = Asp/Glu, blue = Arg/Lys, beige = polar or hydrophobic residues. The avian IDD is 33 amino acids longer (underlined), comprising a hydrophobic hexapeptide (H) followed by a 27 amino acid repeat sequence (182−188) replicating the sequence (149−175). (B) Intensities ratios of free and bound *hu*ANP32A. NP was added to 100 μM ^{15}N *hu*ANP32A at 1:0.05 (blue), 1:0.1 (green), and 1:0.2 (red/brown) ratio (BEST-TROSY at 850 MHz). Bars show intensity ratio with respect to the free spectrum. (C) BEST-TROSY (700 MHz) of free 200 μM of ^{15}N *ch*ANP32A, (red) and at a 1:0.5 molar ratio of NP (blue). (D) BEST-TROSY (850 MHz) of free ^{15}N *hu*ANP32A at 100 μM (red), and at a 1:0.2 (green) and 1:0.5 (blue) molar ratio of NP.

https://doi.org/10.1021/jacs.3c06965
J. Am. Chem. Soc. 2023, 145, 20985−21001

acids, the length of the insertion, in *hu*ANP32A and *ch*ANP32A. The interaction is strongest in the avian form, where it is distinct from the 627(E)-NLS binding site, allowing both viral proteins to bind simultaneously on the same disordered chain, forming a ternary complex. In the shorter, human form, the two interaction sites collapse, so that the NP binding site precisely overlaps the 50 amino acid disordered stretch implicated in binding 627(K)-NLS. Despite this apparent overlap, NMR demonstrates the formation of a ternary complex, stabilized by multivalent interactions between *hu*ANP32A IDD and basic surfaces on both NP and 627(K)-NLS. On the basis of these results, we propose that ANP32A plays the role of an adaptor protein that can colocalize NP and FluPol, possibly for efficient encapsidation and stabilization of newly synthesized RNA. Consideration of the intrinsic flexibility of the interacting domains of ANP32A and FluPol reveals that ANP32A can position NP in the putative RNA exit channel in both FluPol:*hu*ANP32A and FluPol:*ch*ANP32A complexes. The data demonstrate that while deletion of the 33 amino acid segment in *hu*ANP32A abrogates the ability to colocalize NP and FluPol using separate binding sites, by mutating E627 to K, FluPol acquires the ability to interact multivalently in an electrostatically driven ternary complex with the acidic disordered domain of *hu*ANP32A.

RESULTS

Isothermal Titration Calorimetry of NP Interaction with Avian and Human ANP32A. Interaction between the monomeric mutant of H17N10 (A/little yellow shouldered bat/Guatemala/060/2010) NP and *hu*ANP32A and *ch*ANP32A was initially investigated using ITC (Figure S1). The interaction with *ch*ANP32A (120 nM) is approximately 1 order of magnitude stronger than *hu*ANP32A (1.7 μM). The enthalpic contribution is very similar in both cases, with the difference lying predominantly in the increased entropic component. These affinities are notably stronger than those measured for the 627-NLS domains of FluPol, which were estimated from NMR to lie in the 10s to 100s of micromolar range.[32] A similar affinity of *hu*ANP32A for the R416A monomeric mutant nucleoprotein of the A/WSN/33(H1N1) was determined (1.8 μM, data not shown). The latter nucleoprotein was used for NMR experiments for reasons of stability.

NMR Reveals a Shift in the NP Interaction Site between Avian and Human ANP32A. We investigated the interaction of ANP32A with the R416A monomeric mutant nucleoprotein of the A/WSN/33(H1N1) virus NP (hereon referred to simply as NP) using NMR spectroscopy (Figure 2). Titration of NP into ^{15}N labeled *ch*ANP32A results in localized reduction in intensity of peaks, with maximal reduction around ^{210}EEYDEDAQVV^{219}, but extending from 200 to 250. Direct interaction appears to be confined to the IDD, with negligible chemical shifts and uniform, weak broadening in the folded domain. No chemical shifts are observed in the center of the binding region, with almost complete disappearance of peaks in this region at 1:0.5 admixture of NP, in agreement with the tight binding observed by ITC. Intensities in this region report on the residual free *ch*ANP32A in slow exchange between free and bound peaks, with bound peaks not visible due to the high molecular mass of the complex. Small shifts (e.g., 230E, 233E, 237S, or 247Y) are observed in the peripheral regions associated with peaks in intermediate or fast exchange between free and bound protein.

Titration of NP into ^{15}N labeled *hu*ANP32A results in a similar intensity profile, in this case shifted approximately 33 residues downstream, stretching from 169 to 221 and with the largest effects in the region ^{177}EEYDEDAQVV^{186}, a sequence that is identical to residues 210−219 in *ch*ANP32A. Small chemical shifts are observed as a function of admixture, accompanied by significant line broadening, suggesting intermediate exchange on the NMR time scale. Signal from the folded domain is further decreased compared to *ch*ANP32A interaction, possibly due to closer proximity of the binding site to the folded domain.

NP Binds ANP32A via the RNA Binding Pocket. In order to investigate the possible binding interface on the surface of NP, we titrated poly-UC RNA into the *hu*ANP32A:NP complex. This results in return of the intensity of the broadened ANP32A residues to the intensity of the free form, indicating that ANP32A and RNA binding is competitive, and implying that ANP32A binds in the RNA binding groove of NP (Figure 3). Similar conclusions have

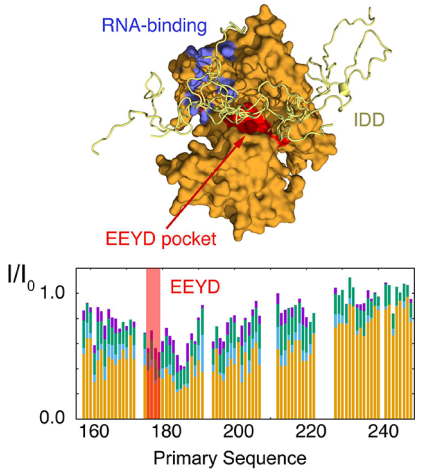

Figure 3. ANP32A IDD appears to bind in the RNA-binding pocket of NP. Histogram shows intensity recovery broadened resonances of ^{15}N *hu*ANP32A (25 μM) bound to H1N1 NP (1:1) upon addition of poly UC RNA 16mer. Yellow, *hu*ANP32A:NP (1:1); blue, 200% RNA; green, 400% RNA; purple, 800% RNA. Cartoon, model of the IDD of *hu*ANP32A bound to NP; blue, the RNA binding grooves identified by Tang et al.;[49] red, the binding pocket locating the EEYD C-terminal peptide of NP.

been drawn from recent studies using pull-down assays of mutated NP with *hu*ANP32A, *hu*ANP32B, and *ch*ANP32A.[47] We note that a linear motif present in the ANP32A binding interface (EEYD) shares sequence identity with the conserved C-terminal NP peptide that binds on the opposite side of the RNA binding groove of NP, again supporting the suggestion that the negatively charged IDD of ANP32A binds the RNA binding groove of NP.[48,49]

***ch*ANP32A Simultaneously Binds NP and *av*627-NLS via Distinct Binding Sites.** In order to determine whether *ch*ANP32A can bind both NP and 627(E)-NLS, we titrated 627(E)-NLS into the *ch*ANP32A:NP complex. The affinity of the complex between *ch*ANP32A IDD is sufficiently tight that it is possible to study the 1:1 complex at a concentration of 100 μM, essentially in the absence of the free forms of the proteins. Titration of 627(E)-NLS into this bimolecular complex resulted in almost identical shifts to those observed in the absence of NP (Figure 4),[32] with chemical shift perturbations

https://doi.org/10.1021/jacs.3c06965
J. Am. Chem. Soc. 2023, 145, 20985−21001

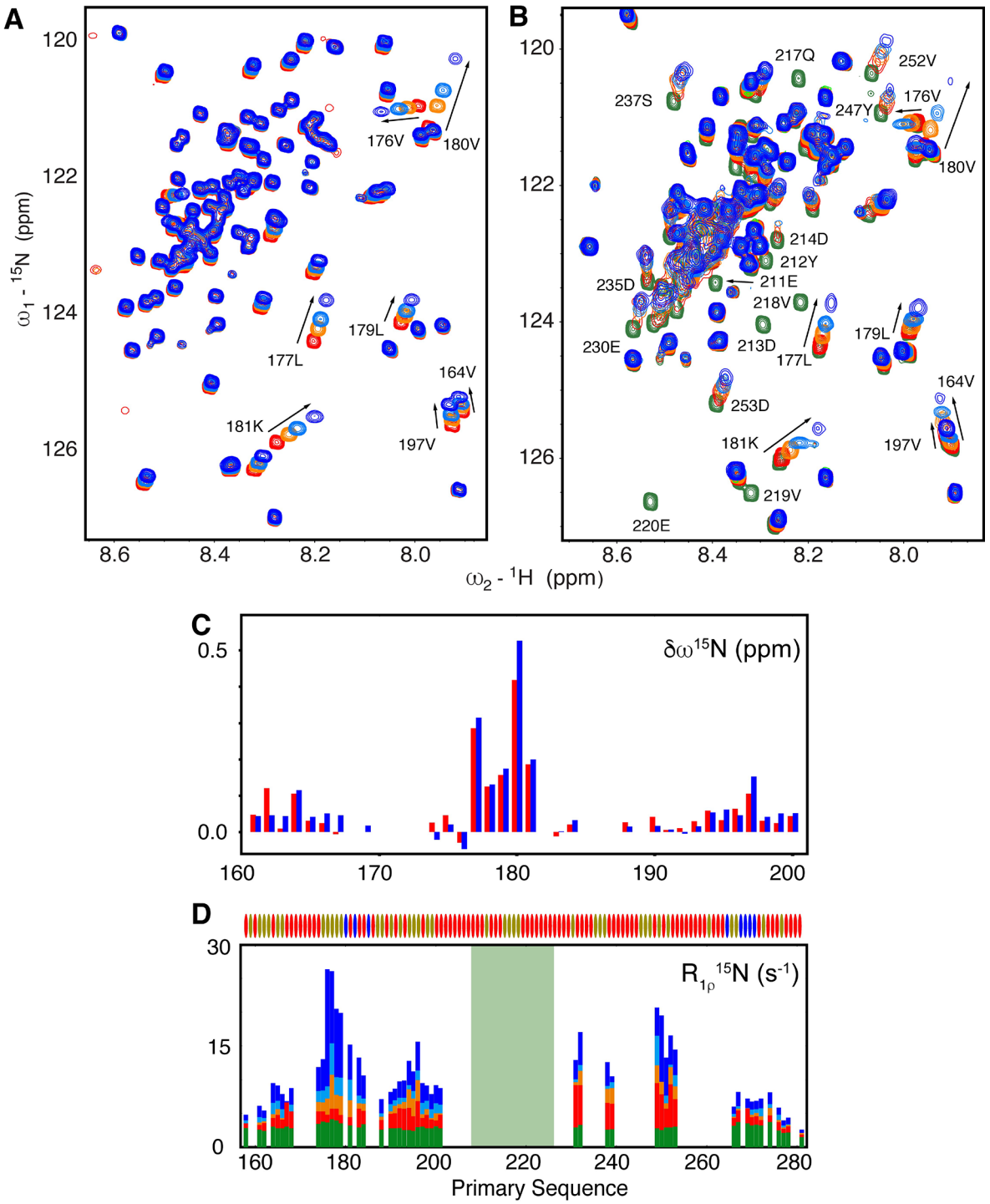

Figure 4. *ch*ANP32A IDD can simultaneously bind 627(E)-NLS and NP via two distinct binding sites. (A) Chemical shifts induced by titration of 627(E)-NLS into *ch*ANP32A IDD (25 μM). Red, free *ch*ANP32A(IDD); orange, 100%; light blue, 200%; dark blue, 400% 627(E)-NLS. These experiments were performed at 200 mM NaCl.[32] Spectra recorded at 850 MHz. (B) Chemical shifts induced by titration of 627(E)-NLS into *ch*ANP32A(IDD):NP 1:1 admixture (25 μM). Green, free *ch*ANP32A(IDD); red, 1:1 *ch*ANP32A(IDD):NP admixture; orange, 100% 627(E)-NLS; light blue, 200% 627(E)-NLS; dark blue, 400% 627(E)-NLS. Spectra recorded at 850 MHz. (C) ^{15}N chemical shift differences between the 0% and 200% admixtures shown in A and B. Blue, *ch*ANP32A(IDD):627(E)-NLS; red, *ch*ANP32A(IDD):NP:627(E)-NLS. (D) $R_{1\rho}$ (850 MHz) of free *ch*ANP32A(IDD) (green); *ch*ANP32A(IDD):NP (1:1) (red); *ch*ANP32A(IDD):NP:627(E)-NLS (1:1:1) (orange); *ch*ANP32A-(IDD):NP:627(E)-NLS (1:1:2) (light blue); *ch*ANP32A(IDD):NP (1:1:4) (dark blue).

(CSPs) again centered on the hexapeptide unique to *ch*ANP32A and part of the section that is deleted in *hu*ANP32A. This demonstrates that binding of 627(E)-NLS and NP to the two interaction sites on *ch*ANP32A, separated by 33 amino acids, is independent and can occur simultaneously, providing a molecular mechanism for colocalizing the two viral proteins via the host adaptor *ch*ANP32A. Spin relaxation ($R_{1\rho}$) measured as a function of 627(E)-NLS admixture shows increasing relaxation in the peripheral regions (resonances from the interaction site are broadened beyond

https://doi.org/10.1021/jacs.3c06965
J. Am. Chem. Soc. 2023, 145, 20985−21001

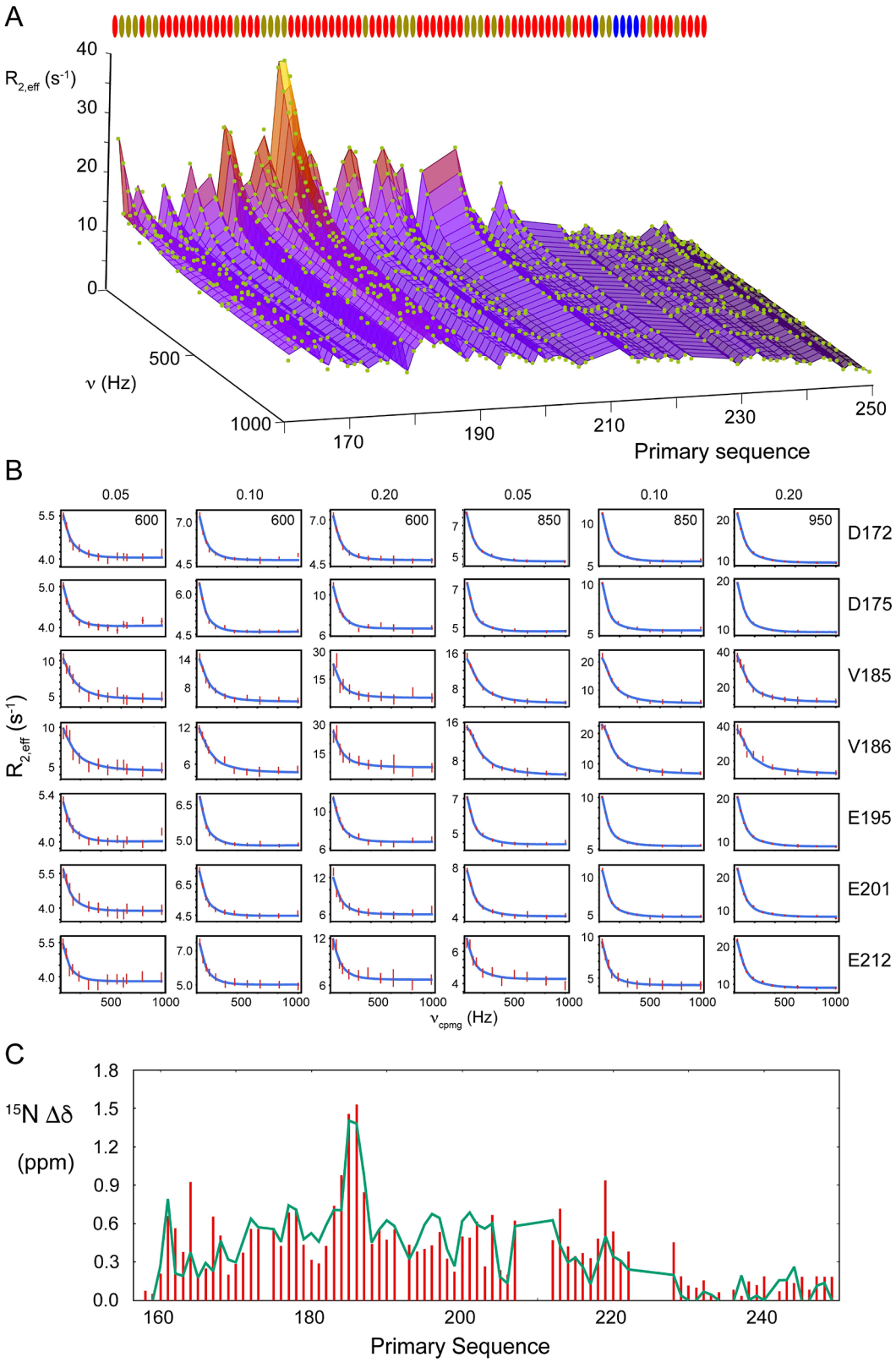

Figure 5. *hu*ANP32A binds NP and 627(K)-NLS via the IDD. (A) Relaxation dispersion measured throughout the IDD of *hu*ANP32A (950 MHz). Data points are shown as green dots. The surface represents the simultaneous fit of all experimental data shown to a single 2-state exchange model (here the 20% admixture of NP is shown in 100 μM *hu*ANP32A). The three-dimensional representation shows CPMG frequency, $R_{2,eff}$ and primary sequence on three orthogonal axes. The color code represents $R_{2,eff}$. (B) CPMG relaxation dispersion profiles of 100 μM ANP32A in the presence of 5%, 10%, and 20% of NP showing selected residues from the region (172−212), measured at 600, 850, and 950 MHz as labeled. The entirety of data sets and fits are shown in Figure S3. (C) Comparison of chemical shift differences between the free and bound form of *hu*ANP32A when it interacts with 627(K)-NLS (red) and NP (green). The former is derived from peak shifts from $^{15}N-^{1}H$ HSQC spectra reporting on fast exchange, while the latter is extracted by fitting of CPMG relaxation dispersion data reporting on intermediate exchange.

https://doi.org/10.1021/jacs.3c06965
J. Am. Chem. Soc. 2023, 145, 20985−21001

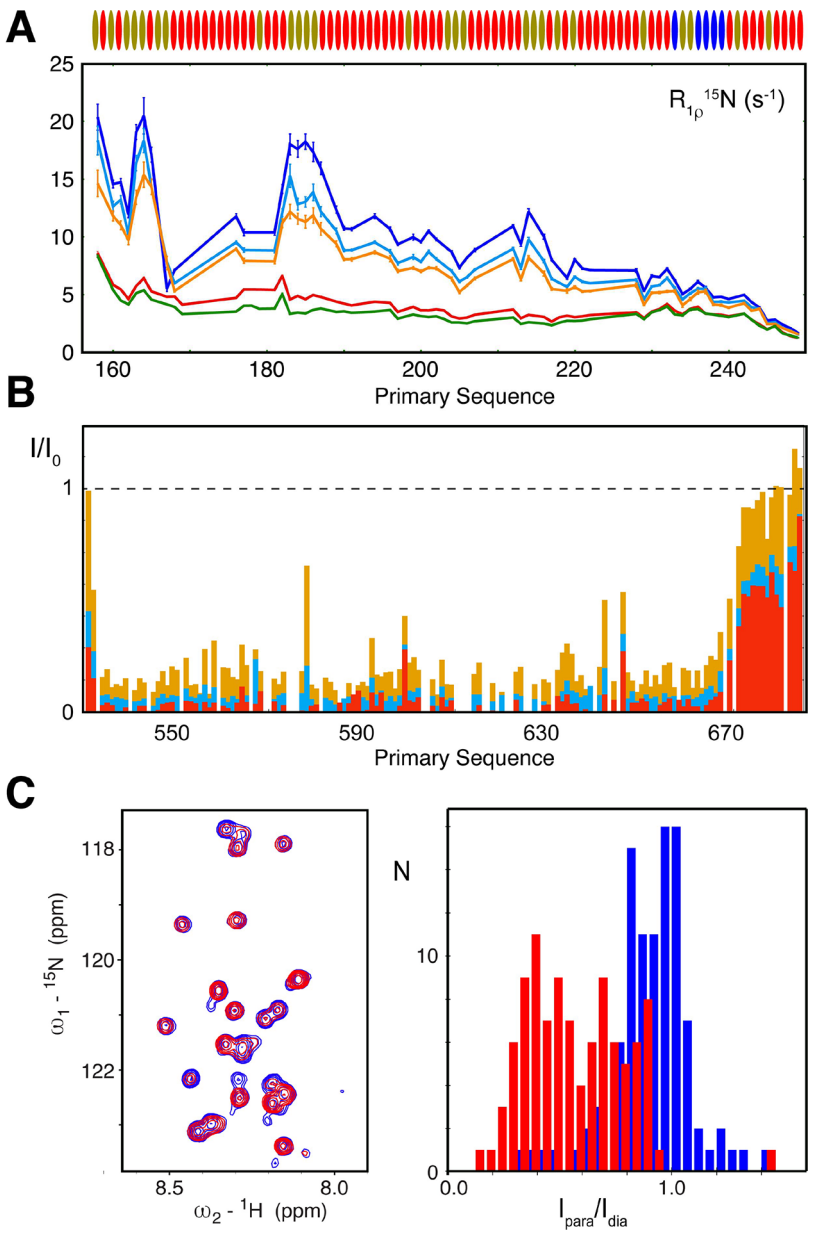

Figure 6. *hu*ANP32A forms a ternary complex with 627(K)-NLS and NP via the same binding interface. (A) Residue-specific ^{15}N $R_{1\rho}$ of 100 μM *hu*ANP32A in free form (green), in the presence of 10 μM NP (red), in the presence of 100 μM (orange) and 200 μM (light blue) 627(K)-NLS, and in the presence of 10 μM NP as well as 200 μM 627(K)-NLS (blue), demonstrating a clear increase in rotational correlation time as the ternary complex is formed. (B) Intensity ratios of ^{15}N−^{1}H HSQC peaks of 100 μM 627(K) relative to the free form, in the presence of 100 μM *hu*ANP32A IDD (1:1:0, orange), in the presence of 100 μM *hu*ANP32A IDD and 100 μM NP (1:1:1, blue), and in the presence of 100 μM *hu*ANP32A IDD and 200 μM NP (1:1:2, red). This again demonstrates that addition of NP does not compete with *hu*ANP32A binding. (C) ^{15}N−^{1}H TROSY spectra and paramagnetic/diamagnetic intensity ratios of ^{15}N labeled 100 μM NP with 100 μM 627(K) with a paramagnetic TEMPO label at residue 631, in the presence (red) and absence (blue) of 100 μM *hu*ANP32A IDD. Distribution of extracted values of I_{para}/I_{dia} for 100 resolved peaks is shown in histogram form (the peaks are not assigned).

detection as expected for a tightly bound complex of this size), further substantiating the observation of simultaneous binding of the two viral proteins and thereby formation of a ternary complex (Figure 4). We note the existence of additional CSPs in these peripheral regions, possibly due to folding back of this region onto 627(E)-NLS bound at the main binding site.

NMR Exchange Identifies the Same Interaction Profile for NP and 627-NLS in Human ANP32A. The suggestion of intermediate exchange in the *hu*ANP32A:NP interaction is verified by the measurement of ^{15}N CPMG relaxation dispersion (Figure 5A,B), confirming the extensive interaction profile apparent from the intensity ratio (Figure 2) demonstrating that the interaction affects a stretch of more than 50 amino acids. Data measured at two magnetic fields as a function of NP admixture (0, 5, 10, and 20%) are highly consistent, with the difference in ^{15}N chemical shifts between free and bound states, over the entire region of *hu*ANP32A involved in the interaction agreeing very closely at all admixtures (Figure S2). All data from each individual admixture can be fitted to a 2-state process (Figure S3), providing an estimation of the population of the bound state at each admixture, revealing site-specific affinities in the 50 μM

https://doi.org/10.1021/jacs.3c06965
J. Am. Chem. Soc. 2023, 145, 20985−21001

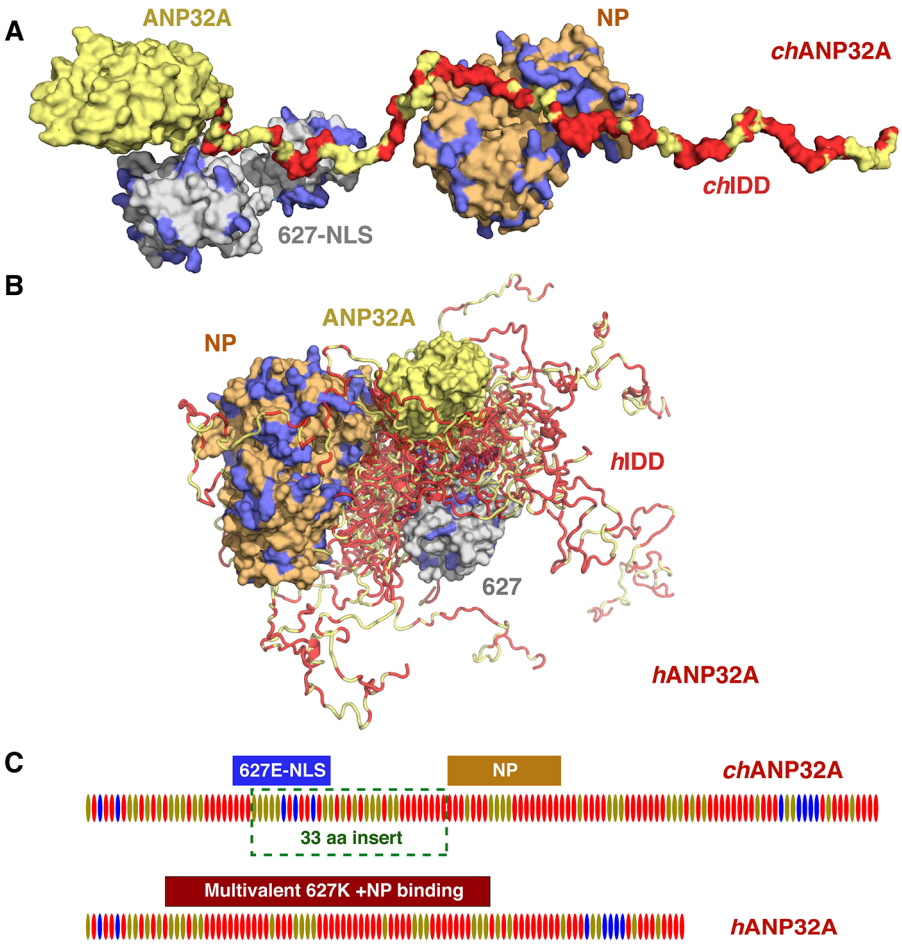

Figure 7. Mutation of the 627 domain allows FluPol to adopt a differential binding strategy to compensate the absence of distinct NP/627-NLS binding sites on *h*ANP32A. (A) Illustration of simultaneous binding of *ch*ANP32A (yellow) IDD (red shows positions of acidic residues) to 627(E)-NLS (gray) and NP (orange) using the distinct binding sites characterized in Figure 4A−D. Positions of positively charged residues in NP and 627(E)-NLS are shown in blue. (B) Multiconformational representation of the interaction of *hu*ANP32A IDD (red/yellow) with both NP (orange/blue) and the 627(K) domain of FluPol (gray/blue) as revealed by data shown in Figures 5 and 6A−C. Positions of charged residues in NP and 627(E)-NLS are shown in blue (positive) and ANP32A IDD in red (negative), respectively. (C) Top, main binding sites of 627(E)-NLS and NP on *ch*ANP32A IDD (boxes identify regions with the largest CSPs upon addition of 627(E)-NLS and regions showing disappearance of peaks upon addition of NP). Bottom, extended simultaneous, multivalent binding site of 627(K)-NLS and NP on *h*ANP32A IDD (box identifies extent of CSPs and relaxation dispersion profiles shown in Figure 5C).

range. This is in contrast to the affinity measured for the entire molecular system from ITC (1.7 μM), again indicating a strong component of multivalency, with interaction sites distributed over the 50 amino acid stretch contributing to the overall affinity. Remarkably, these chemical shift differences are essentially identical, both in magnitude and profile over the sequence, to those induced by interaction with human-adapted 627(K)-NLS (Figure 5C),[32] suggesting that the nature of the interaction is very similar in both cases. The two interactions involve the same long stretch (170−220) of the IDD of *hu*ANP32A, apparently forming polyvalent interactions with the strongly positively charged protein surface on NP or 627(K)-NLS.

***hu*ANP32A Simultaneously Binds NP and 627(K)-NLS via the Same Binding Site.** The observation of simultaneous binding of NP and 627(E)-NLS to *ch*ANP32A, and the possible relevance of this ternary complex for colocalization of viral FluPol and NP in replication, poses the obvious question of whether *hu*ANP32A can colocalize NP and 627(K)-NLS. This is particularly intriguing given the apparently identical CSPs induced by both partners, suggesting that the identical region along the disordered strand of *hu*ANP32A binds to NP and 627(K)-NLS.

Addition of NP and 627(K)-NLS results in increase in transverse relaxation rates measured on *hu*ANP32A, as expected upon formation of the two binary complexes, with *hu*ANP32A being close to saturation in the 1:2 *hu*ANP32A:627(K)-NLS complex. Addition of NP (10%) to this mixture results in an increase in transverse relaxation of *hu*ANP32A which is significantly and systematically higher than either of the two binary complexes (Figure 6A). This suggests the existence of a cooperative binding mode rather than competition between the bimolecular interactions of NP and 627(K)-NLS with *hu*ANP32A. While it is not possible on the basis of these data to estimate the correlation time of such a ternary complex, due to unknown stoichiometry and relative affinity, the most probable explanation for the higher relaxation rate is the simultaneous colocalization of all three proteins in a ternary complex. The same effect is observed for exchange-free relaxation measured using cross-correlated CSA-dipole cross-relaxation (η_{xy}) (Figure S4) indicating that this phenomenon is also not due to exchange contributions to R_2 (that do not

https://doi.org/10.1021/jacs.3c06965
J. Am. Chem. Soc. 2023, 145, 20985−21001

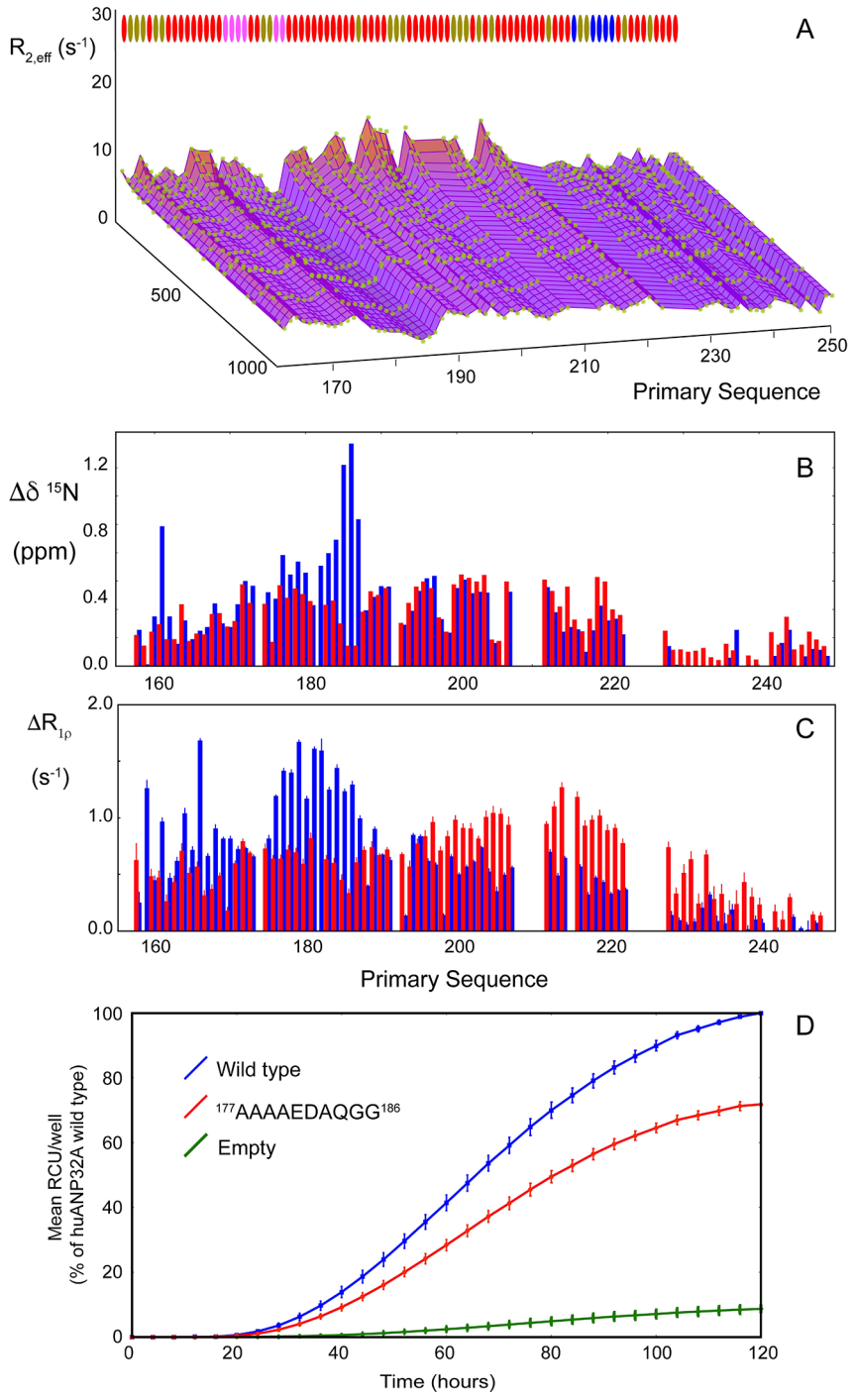

Figure 8. Relaxation and relaxation dispersion confirm the multivalent nature of the *hu*ANP32A:NP interaction. (A) CPMG relaxation dispersion profile of 100 μM *hu*ANP32A throughout the IDD (^{177}AAAAEDAQGG^{186}, mutated residues are shown in pink) in the presence of 10 μM NP, measured at 850 MHz. Data points are shown as green dots. The surface represents the simultaneous fit of all experimental data shown to a single 2-state exchange model. The three-dimensional representation shows CPMG frequency, $R_{2,eff}$, and primary sequence on three orthogonal axes. The color code represents $R_{2,eff}$. (B) Residue-specific chemical shift differences between the free and bound form of WT (blue bars) and mutant *hu*ANP32A(^{177}AAAAEDAQGG^{186}) (red bars) (both 100 μM), in the presence of 10 μM NP, as determined from relaxation dispersion measured at 600 and 850 MHz. All sites were fit simultaneously to a 2-state exchange model using ChemEx ($p_B = 0.70 \pm 0.01$, $k_{ex} = 270 \pm 11$ s^{-1}). (C) Residue-specific ^{15}N $R_{1\rho}$ (700 MHz) differences of *hu*ANP32A in the presence and absence of 10 μM NP; *hu*ANP32A WT (blue bars) and *hu*ANP32A(^{177}AAAAEDAQGG^{186}) (red bars). (D) Cellular influenza polymerase activity in the absence of ANP32A/B (green), and in the presence of *hu*ANP32A-wt (blue), and *hu*ANP32A ^{177}AAAAEDAQGG^{186} (red), corresponding to the mutation investigated *in vitro*. A/WSN/1933 FluPol activity was measured by vRNP reconstitution in HEK-293T ANP32AB KO cells by transient transfection using a model vRNA encoding mCherry as well as either *hu*ANP32A wild-type (WT) or *hu*ANP32A mutants. Fluorescence signals were acquired every 4 h and are represented as RCU × μm^2/Well ± SD of three experiments performed in triplicate.

https://doi.org/10.1021/jacs.3c06965
J. Am. Chem. Soc. 2023, 145, 20985−21001

contribute to η_{xy}). We note that no direct interaction was observed between NP and 627(K).

Further evidence to support the existence of a ternary complex is provided by observing signals from ^{15}N-labeled 627(K) in complex with unlabeled *hu*ANP32A. In the presence of *hu*ANP32A, the folded region of 627(K) uniformly lose intensity, presumably due to the increased correlation time of the complex (Figure 6B). Upon addition of NP to this mixture, signals of 627(K) further lose intensity rather than increasing as would be expected if 627(K) were released due to competitive binding of NP.

Finally, we observe approximately 100 ^{15}N−^{1}H TROSY cross peaks from the third component protein, NP. Although these are currently unassigned, they can be used to investigate the existence of contacts between NP and ANP32A and 627-NLS by paramagnetically labeling 627(K) (at residue 631). We measured negligible line-broadening in NP spectra due to the presence of paramagnetic 627(K), confirming the lack of direct interaction with NP. However, when the experiment was repeated in the presence of both 627(K) and *hu*ANP32A IDD(1:1:1), extensive paramagnetic broadening of numerous NP peaks was observed (Figure 6C), confirming that a significant population of 627(K) and NP is only in close proximity when *hu*ANP32A IDD is present. This verifies the observation that ANP32A is essential to colocalize the two viral factors and again directly demonstrates the existence of the ternary complex.

NMR relaxation and paramagnetic relaxation experiments from all three component proteins unambiguously confirm the formation of a ternary complex, mediated by the common extended interaction epitope on *hu*ANP32A. We previously identified the interaction between *hu*ANP32A and 627(K)-NLS as multivalent,[32] on the basis of the very different site-specific affinities measured when observing *hu*ANP32A (600 μM) or 627(K)-NLS (20 μM), and the multiplicity of contacts along the extensive acidic binding interface on *hu*ANP32A interacting with the basic surface of 627(K)-NLS. Here we show that a similar phenomenon applies to the binding of NP, where relaxation dispersion identifies the identical extended binding sites on *hu*ANP32A, and a nearly 20-fold difference in affinity when observing the overall K_D and the local affinity determined for each site.

The most likely scenario explaining these data measured on all three partners is that the ternary complex exploits multivalent interactions between the acidic IDD of *hu*ANP32A and the basic surfaces of 627(K)-NLS and NP, thereby colocalizing both viral partners via the host adaptor protein. This novel interaction mode compensates the disappearance of the 627(E)-NLS binding site present in *ch*ANP32A, and provides a physical explanation for the crucial impact of the E627K mutation on adaptation.

Distinct Ternary NP:ANP32A:627-NLS Complexes in Human and Avian Adapted Environments. The conformational samplings of 627-NLS and ANP32A have been previously described in detail in the case of both human-adapted and avian-adapted binary complexes.[32] Here we investigate the steric feasibility of the proposed ternary complexes, incorporating NP in addition to the bound 627-NLS domains. Assuming the broad interaction interface comprises the *ch*ANP32A peptide ^{210}EEYD^{213} bound in the RNA binding groove, it is evident that despite extensive interaction surfaces, both viral partners can simultaneously bind *ch*ANP32A IDD via distinct main interaction motifs (Figure 7A,C). Representing the human-adapted complex poses a more challenging problem, requiring the depiction of multivalent interactions involving both NP and 627(K)-NLS with *hu*ANP32A. The nature of the observed multivalency strongly suggests a highly dynamic complex, involving interaction sites distributed along the region between 170 and 220 binding and unbinding rapidly to both partners, thereby maintaining the colocalization of *hu*ANP32A with 627(K)-NLS or NP simultaneously in the ternary complex. In particular NP and 627-NLS need to be close enough to allow for paramagnetic broadening of residues on the surface of NP by the TEMPO label attached to residue 631 in 627(K) (Figure 7B,C). These putative multiconformational models are presented to demonstrate the steric feasibility of such a ternary complex and to illustrate the rapid interchange between multivalent contact points that maintains ternary colocalization.

Mutation Studies Confirm the Multivalent Nature of the *hu*ANP32A:NP Interaction. The multivalent nature of the interaction is supported by the observation that mutation of the apparent interaction hotspots (as measured from the magnitude of the CSP), ^{178}EEYDEDAQVV^{185} to ^{178}AAAAED-AQGG^{185} do not abolish the interaction as observed on the remaining residues in the interaction interface. Relaxation dispersion is measured throughout the interaction interface (Figure 8A), revealing similar chemical shift differences as measured in the wild-type protein for the nonmutated residues (Figure 8B). Interestingly, the mutation increases transverse relaxation rates in the downstream 200−220 region, suggesting a compensatory increase in the population of the remainder of the bound state upon mutation of these motifs (Figure 8C). These data substantiate a model in which none of the individual linear motifs participating in the multivalent interaction is essential and that each contributes to the overall affinity.

Cellular assays were carried out to measure polymerase activities using ANP32A/B knockout HEK293T cells complemented with transiently expressed wild-type or ^{178}EEYDEDAQVV^{185} to ^{178}AAAAEDAQGG^{185} mutated *hu*ANP32A, in a standard vRNP reconstitution assay using a viral model RNA encoding mCherry. Monitoring of mCherry fluorescence, measured as a function of time post-infection, demonstrates that while polymerase activity is maintained (consistent with studies *in vitro*) its overall efficiency is slightly reduced in the mutated form. This suggests, possibly not surprisingly, that the increased binding of the downstream region in the presence of these mutations is only partially compensating the defect in supporting polymerase activity.

NP:ANP32A:627-NLS Ternary Complexes in the Context of the Full-Length Replicase/Encapsidase. It is evident that the conformational space available for NP bound to ANP32A will be modified in the context of full-length FluPol. In this context, we have modeled the conformation of a dimeric form of FluPol from IAV bound to ANP32A using the recent structure of FluPol Influenza C.[37] Following the proposition of Carrique et al., nascent RNA is threaded from the replicase FluPol active site via the proposed RNA exit channel to the encapsidase FluPol where the 5′ RNA is tethered (Figure 9A,B). The synthesized RNA is then solvent accessible in the exit channel. We note that the relative position of the folded domain of ANP32A and the 627 domain in both solution ensembles of 627-NLS and ANP32A is similar to the relative conformation of ANP32A and the encapsidase

https://doi.org/10.1021/jacs.3c06965
J. Am. Chem. Soc. 2023, 145, 20985−21001

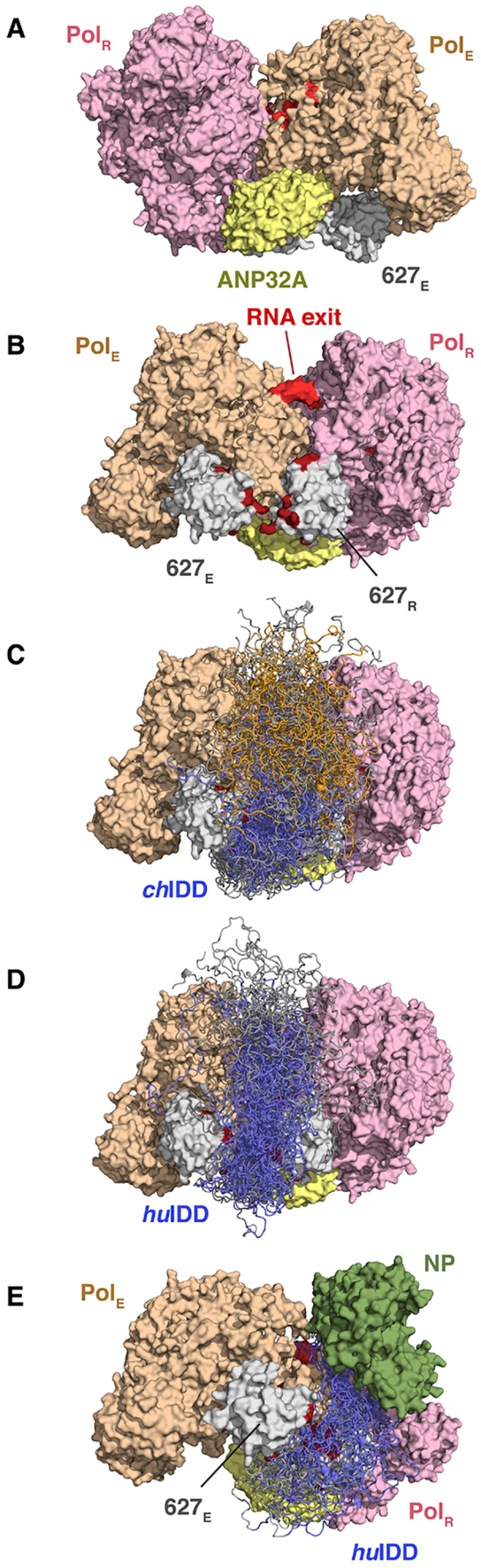

Figure 9. Modeling the ternary complexes of ANP32A in the context of the dimeric FluPol replicase. (A) The conformation of the replicase/encapsidase FluPol dimer was modeled on the basis of the Influenza C structure determined by Carrique et al.[37] Synthesized RNA was threaded from the replicase FluPol (pink) via the proposed RNA exit channel to the encapsidase FluPol (orange). The exit point of the synthesized RNA (red) is then solvent accessible, as seen in the rotated conformation (B). ANP32A folded domain (yellow) is located in the equivalent position as determined for Influenza C. The two 627 domains corresponding to the replicase (627_R) and the encapsidase (627_E) are shown in gray, with the ANP32A binding residues shown in dark red. (C) Ensemble representation of the conformational sampling of the disordered domain of *ch*ANP32A (*ch*IDD) (calculated using flexible-meccano). Conformers shown all fulfill the constraints that the 627(E)-binding region (blue, the region 175−195, including the hexapeptide) is in the vicinity (<15 Å) of one of the 627 domains, while the NP binding motif (orange, 205−225) is within 40 Å of the exit point of the newly synthesized RNA (thereby allowing NP to bind the emergent RNA). This suggests a plausible mechanism to place NP adjacent to nascent RNA, while locating the 627(E)-NLS binding site, 33 amino acids upstream, to the surface of 627(E)-NLS (Figure 7C). (D) The equivalent *hu*ANP32A complex in the same context. The extended 627(K) and NP binding motif (blue), from 170:220, can sample conformations within 40 Å of the RNA exit point as well as either 627_R or 627_E. (E) NP (green) was placed in the bottom of the exit channel, to illustrate the ability of the extended binding motif of *hu*ANP32A to locate NP within 40 Å of the RNA exit point, while interacting with $627_R/627_E$.

627 domain, suggesting that this orientation is predominant in the minimal complex studied in solution. The conformational space available to the IDD in the context of this model was calculated using flexible-meccano,[50,51] allowing us to investigate the possible sampling radius of ANP32A and the relevance of the proposed ternary complexes within this structural context. Assuming that NP binds 24 nucleotides of the newly synthesized RNA in the groove between FluPol$_R$ and FluPol$_E$, we impose a minimum distance of 40 Å between the respective binding regions on *hu*ANP32A and *ch*ANP32A and RNA as it exits FluPol$_R$. In the case of avian ANP32A, the NP-binding site can clearly reach the putative RNA exit channels, suggesting a plausible mechanism for locating NP to nascent RNA, while locating the 627-NLS binding site, 33 amino acids upstream, to the surface of the adjacent 627-NLS domains of the replicase and encapsidase (Figure 9C).

The equivalent *hu*ANP32A complex with FluPol can be modeled in a similar fashion. In this case, we investigated whether the extended binding motif can sample conformations within 40 Å of the RNA exit position, while interacting with the 627 domains, revealing that this is indeed the case, placing NP at the base of the broadly defined RNA exit channel (Figure 9D). In order to accommodate this restraint, the ANP32A IDD is required to pass in the vicinity of the previously identified interaction surfaces of FluPol$_R$ and FluPol$_E$ 627 domains, comprising residues 587, 591, 627, and 631, all amino acids whose mutation has been associated with pandemic strains, and which show enhanced interaction in the *hu*ANP32A:627(K)-NLS complex compared to the *ch*ANP32A:627(E)-NLS complex.[32] This also correlates closely with the observation of electron density between basic residues on the two closely positioned 627 domains in the influenza C dimer, density which was assigned to the acidic *hu*ANP32A IDD.[37] In order to determine whether NP can be accommodated in this molecular assembly, we have positioned NP in the bottom of the RNA binding cleft (at 40 Å from the

https://doi.org/10.1021/jacs.3c06965
J. Am. Chem. Soc. 2023, 145, 20985−21001

initial RNA exit point), demonstrating that amino acids on the common binding epitope on *hu*ANP32A can intercalate between $FluPol_R$ and $FluPol_E$ 627-NLS domains and NP, and supporting the plausibility of such a preassembly configuration (Figure 9E).

DISCUSSION

The interaction between IAV FluPol and members of the host transcription factor ANP32 family has been shown to be essential for viral replication,[7,20,23,25−29] although its function is not yet understood. In particular, the presence of a 33-amino acid deletion in the human forms of the protein has been shown to drive adaptation of FluPol, via E627K or other amino acids on the surface of the 627-NLS domains, so that avian FluPol can function in human cells.[20] The molecular function of ANP32 in viral replication is not known, although it has been shown to interact with both NP and FluPol, suggesting a role related to paramyxoviral phosphoproteins, essential viral cofactors that traffic nucleoproteins to the RNA replication-transcription complexes.[47,52−55] Our recent study described the highly dynamic bimolecular complexes between human and avian ANP32A and human and avian adapted 627-NLS domains of FluPol, revealing distinct binding modes.[32] The human complex exploits extensive multivalency, involving electrostatic interactions dispersed along the length of the highly acidic IDD and the 627 domain where the E627K mutation creates a continuous electrostatic surface. This kind of highly multivalent interaction involving IDPs has been observed throughout biology,[56−58] for example, between electrostatically complementary nuclear proteins,[59,60] in the nuclear pore, involving short linear motifs,[61] and playing a role in the stabilization of membraneless organelles.[62] The avian complex on the other hand was found to be stabilized by interactions involving the avian-specific hexapeptide in the avian ANP32A IDD, binding to 627(E)-NLS, and no direct evidence for multivalency was detected.

Here we further investigate the role of ANP32A in IAV replication by describing the interactions of NP with avian and human ANP32A. NP interacts with the IDDs of ANP32A, via an extended binding site comprising a peptide motif (EEYD) that is also present in the C-terminal tail of NP, and that likely binds in the RNA binding cleft, as previously proposed.[47] The NP interaction site on ANP32A is shifted by 33 amino acids between human and avian forms, which corresponds to the length of the avian-specific insertion. In the avian case, we show that NP interaction is fully compatible with binding of 627(E)-NLS, allowing the two viral proteins to colocalize simultaneously on the IDD, forming a ternary hub-like complex.

NP binding to *hu*ANP32A is an order of magnitude weaker (1.7 μM) and in intermediate exchange on the NMR time scale, allowing us to precisely characterize the structure, kinetics, and thermodynamics of the interaction using NMR exchange methods. This reveals that an extended stretch of more than 50 amino acids are involved in the interaction interface, with an effective site-specific affinity of around 50 μM. This indicates that, similarly to the 627(K) domain, ANP32A also binds NP multivalently via multiple interaction sites along the chain, whose individual affinities are significantly weaker than the collective affinity for the entire protein. Most remarkably, the chemical shift differences induced by the interaction are essentially identical to those measured on the same protein upon interaction with the 627(K)-NLS domains of FluPol, both in amplitude and exact distribution along the primary sequence.

Despite the similarity of the binding profiles, NMR relaxation of ANP32A measured in the presence of both partners reveals the formation of a ternary complex, capable of significantly slowing the rotational correlation times. In addition, 627(K) resonances broadened due to addition of ANP32A are further broadened upon addition of NP, again indicating the absence of competitive (and therefore the apparent existence of simultaneous) binding, while broadening of backbone and side chain resonances of NP, due to the addition of paramagnetically labeled 627(K), is only observed in the presence of ANP32A. These data, individually and collectively, demonstrate the existence of a ternary complex of 627(K)-NLS:*hu*ANP32A:NP, mediated by the same 50 amino-acid stretch of *hu*ANP32A. Remarkably, the IDD is interacting multivalently with both folded viral partner proteins so that fast on and off rates with respect to both proteins allow individual binding sites on the IDD to interact rapidly and transiently with the basic surfaces of the two partners thereby maintaining their dynamic colocalization. This observation reveals the importance of the previously observed multivalent *hu*ANP32A:627(K)-NLS interaction, unique to the human-adapted polymerase, and uncovers the molecular basis of the crucial E627K adaptive mutation, that confers the ability to interact multivalently and thereby enable ternary interaction, despite the absence of the two distinct binding sites that are present in *ch*ANP32A.

This remarkable multivalent nature of the interaction is further supported by investigation of the interaction of NP with *hu*ANP32A mutated at the apparent NP interaction hotspots (^{178}EEYD^{181} and ^{184}VV^{185}). In this case, although interaction at these sites is impacted, binding is enhanced for residues further along the binding region, as expected by increased avidity for these sites due to the absence of the mutated sites. Cellular assays conducted using ANP32A/B knockout HEK293T cells expressing mutated ANP32A also demonstrate that while polymerase activity is affected when the ^{178}EEYD^{181} and ^{184}VV^{185} sites are mutated, it is not abolished. This also testifies to the resilience of this interaction mechanism to variations encountered in mammalian ANP32 IDDs.

Cryo-EM structures show that ANP32A binds to an asymmetric dimer of FluPol from influenza C, bridging across replication and encapsidation-competent FluPols.[37] This dimeric interface was also found in crystal and cryo-EM structures in the absence of ANP32A, suggesting that the host factor is not essential to the structure, although it may stabilize the conformation, in particular because electron density was noted between basic residues on the two closely positioned 627 domains,[37] and this density was assigned to the acidic *hu*ANP32A IDD.

Using this structure as a template, we modeled the replication/encapsidation dimer of IAV, threading an RNA strand from the replicase to the encapsidase. We used this model to explore the possible sampling behavior of the *hu*ANP32A IDD in this molecular context, building the entire disordered chain in agreement with experimental NMR chemical shifts. Simple restraints, requiring simultaneous proximity of *hu*ANP32A residues in the interaction motif with the surface of 627(K) and placing NP at an appropriate distance to the RNA exit channel, demonstrate that the NP:627(K) multivalent interface on the IDD can indeed acts

https://doi.org/10.1021/jacs.3c06965
J. Am. Chem. Soc. 2023, 145, 20985−21001

as an adaptor, colocalizing NP and 627 in the vicinity of newly synthesized RNA prior to encapsidation. We note that in order to fulfill these constraints, the extended binding motif of the *hu*ANP32A IDD must pass in the proximity of the interface between the replicase and encapsidase 627 domains, as previously suggested on the basis of electron density observed in this channel.[37] Not surprisingly, *ch*ANP32A IDD can easily fulfill constraints that place the two interaction motifs in the vicinity of 627(E)-NLS and the putative RNA exit channel, respectively.

FluPol is known to be extremely plastic in solution, as illustrated by the numerous high resolution structures,[63,12,13,5,64,65] where PB2, and the 627-NLS domains in particular, have been shown to either change position relative to the core of FluPol,[13] or to disappear entirely, indicating extensive sampling of conformational space on the surface of FluPol. It is possible that this intrinsic flexibility is maintained in the context of the replicase/encapsidase dimer, providing even more degrees of conformational freedom, for example, if one or both 627 domains, which are stabilized by few interactions with FluPol, dissociate from the surface. Experimental data will be necessary to verify the validity of both the assumptions inherent to this modeling and the true context of the very different interaction mechanisms of *hu*ANP32A and *ch*ANP32A revealed by NMR, but it already seems clear that a degree of convergence exists between the complementary information provided by NMR and cryo-EM.

CONCLUSION

In conclusion, by comparing the ternary complexes of *hu*ANP32A and *ch*ANP32A with NP, we identify two very different interaction mechanisms that provide the key to understanding the molecular basis of adaptive mutations in the C-terminal region of PB2 that are necessary for influenza replication in human cells. While *ch*ANP32A can bind FluPol and NP simultaneously via distinct linear motifs, the deletion in *hu*ANP32A blocks this mode of colocalization in *hu*ANP32A. In order to function, IAV therefore must mutate residues on the surface of 627, completing and enhancing the basic interaction surface, allowing *hu*ANP32A to then simultaneously bind FluPol and NP via the same surface, thereby forming a multivalent ternary complex. The identification of a common, extended motif on the IDD of ANP32A that simultaneously binds both viral proteins hints at possible exploitation of this sequence for the development of potent peptide-based inhibitors of NP and FluPol.

MATERIALS AND METHODS

Constructs. Chicken ANP32a (*Gallus gallus*, XP_413932.3) was synthesized and codon optimized for expression in *E. coli* (GenScript, New Jersey, USA). Human ANP32a was overexpressed using plasmid pQTEV-ANP32a, which was a gift from Konrad Büssow (Addgene plasmid 31563). Plasmids containing just the intrinsically disordered region of chicken (149−281) or human ANP32a (144−249) were cloned into a pET9a derived plasmid with an N-terminal His-tag and a TEV cleavage site (MGHHHHHHDYDIPTTENLYFQG).

A codon-optimized construct containing the 627-NLS domains of the PB2 subunit was synthesized (538−759) from avian H5N1 A/duck/Shantou/4610/2003 (Geneart, Regensburg, Germany) for expression in *E. coli*.[11] A construct containing just the 627 domain (538−693) was cloned into a pET9a plasmid with an N-terminal His-tag and a TEV cleavage site (see above).[32]

The NP gene from strain A/WSN/33 (H1N1) with a His-tag at its C-terminal was cloned in the pET22 plasmid (Novagen). Single point mutation R416A was introduced through the Quick-Change kit (Stratagene) in order to induce monomerization of the protein.[48] The NP H17N10 gene from little yellow-shouldered bat/Guatemala/060/2010(H17N10) was cloned in the pETM11 plasmid with an N-terminal His-tag and a SUMO tag containing a TEV cleavage site. The single point mutation R415A was introduced for monomerization.[48]

Protein Expression and Purification. All proteins were expressed in *E. coli*-BL21 (DE3) Novagen) or AI (Invitrogen). Cultures were grown in LB or M9 media and induced with IPTG for 16 h at 18 °C. Bacteria were harvested by centrifugation and resuspended in buffer A containing Tris-HCl pH 7.5 and 200 mM NaCl (buffer A for NP contained 1 M NaCl). Bacterial lysis was performed by sonication. All proteins were purified by affinity chromatography on Ni-NTA agarose (Qiagen), followed by incubation with TEV protease at 4 °C overnight coupled with dialysis into buffer A.

For NP overexpression, cells were grown in LB or M9 media until the OD600 reaches 0.8−1.0, follow by induction with 0.2 mM IPTG and overexpression for 16 h at 25 °C. Bacteria were harvested and resuspended in a lysis buffer containing Tris-HCl pH 7.4, 300 mM NaCl, 2 mM MgCl2, 15 mM imidazole and RNase A. Bacterial cells were lysed by sonication. Clarified bacterial lysate was then incubated with Ni-NTA agarose (Qiagen) at 4 °C for 30 min. Ni-NTA beads were then washed with 10 column volumes of high salt buffer containing Tris-HCl pH 7.4, 1 M NaCl, 2 mM $MgCl_2$, and 1 mM β-ME. Protein was then eluted with 300 mM Imidazole. The eluent was then dialyzed into Tris-HCl pH 7.4, 300 mM NaCl, and 0.5 mM β-ME, then loaded onto a HiTrap Heparin HP affinity column (Cytiva life sciences). A salt gradient from 300 mM NaCl to 1 M NaCl was used during elution.

For PRE experiments, a single cysteine mutant at position 631 of the 627 domain was tagged using 4-maleimido-TEMPO. Briefly, purified cysteine mutants were reduced with an excess of DTT at 4 °C for 12 h, and then dialyzed into 50 mM phosphate buffer pH 7.0 with 150 mM NaCl and no DTT. Afterward, a 5-fold molar excess of 4-maleimido-TEMPO dissolved in DMSO was added to the reduced protein. The reaction was incubated for 12 h at 4 °C and then excess of TEMPO was eliminated through size exclusion chromatography.

Isothermal Titration Calorimetry. Isothermal titration calorimetry was measured using MicroCal iTC200 (GE healthcare) at 25 °C. Experiments were performed typically by adding 2.5 μL of aliquots of 200 μM of human or chicken ANP32A into the microcalorimeter cell filled with 20 μM of monomeric H17N10 NP; the titration mixture was stirred at 750 rpm. Data were fitted using Origin 7.0 with the ITC plugin from MicroCal.

Nuclear Magnetic Resonance Experiments. All NMR experiments were acquired, unless indicated, in 50 mM Tris-HCl buffer pH 6.5, 50 mM NaCl, and 10% D_2O on Bruker spectrometers with 1H frequencies of 600, 700, 850, and 950 MHz equipped with cryoprobes operating at 20 °C. All spectra were processed using NMRpipe[66] and analyzed in NMRFAM Sparky.[67]

For the RNA competition experiments, TROSY spectra of 1:1 mixtures of 25 μM of ^{15}N *hu*ANP32A with NP were measured in the absence and presence of a 16-mer poly-UC oligonucleotide RNA repeat at a 2-, 4-, or 8-fold excess at 700 MHz.

^{15}N $R_{1\rho}$ relaxation rates were measured at 20 °C using a spin lock of 1.5 kHz.[68] A typical set of relaxation delays included points measured at 1, 15, 30, 50, 70, 120, and 230 ms, including repetition of one delay. Relaxation rates were extracted using in-house software and errors were estimated using a noise-based Monte Carlo simulation. Transverse cross-correlated ^{15}N−^{1}H CSA/DD cross relaxation rates (η_{xy}) were measured as previously described.[69]

Paramagnetic relaxation enhancement effects used to probe the formation of the ternary complex were measured from peak intensity ratios of ^{15}N-TROSY spectra between a paramagnetic and a diamagnetic sample which was incubated with 2 mM ascorbic acid. The samples contained 100 μM ^{15}N-labeled NP (H1N1, 416A) and TEMPO-labeled 627(K), with or without huANP32A (1:1:0 or 1:1:1).

https://doi.org/10.1021/jacs.3c06965
J. Am. Chem. Soc. 2023, 145, 20985−21001

^{15}N CPMG relaxation dispersion experiments[70−72] were acquired at 20 °C using a constant time relaxation delay of 32 ms, a ^{1}H decoupling field of 11 kHz and 14 CPMG frequencies (ν_{CPMG}) ranging from 31.25 to 1000 Hz, including repeats for estimation of uncertainties on peak intensity. Uncertainties on R_{2eff} values were propagated from the peak intensity uncertainty using a Monte Carlo approach. All relaxation dispersion data were analyzed using the program ChemEx (https://github.com/gbouvignies/ChemEx).

Modeling of Ternary Complexes. The recently published complex of ICV FluPol asymmetric dimer,[37] bound to *hu*ANP32A, was used as a template to construct a putative model of an equivalent IAV complex by superposing equivalent domains and modeling the replicase in elongation state, with the 5′ end of the product extending into the encapsidase 5′ hook binding site.

Ensemble descriptions of the ternary complex of *hu*ANP32A:NP:627(K)NLS, accounting for the disordered domain of *hu*ANP32A and *ch*ANP32A, were constructed using the flexible-meccano algorithm,[50,51] which samples conformational space by randomly sampling free-energy surfaces describing the backbone dihedral angles ϕ/ψ for each residue in the disordered domain. Steric hindrance due to the presence of the FluPol domains, NP, and the bound RNA are accounted for using hard sphere repulsion. Reasonable constraints were used to restrict conformational space to test certain selected scenarios. Namely, (a) the IDD of the binding region of *hu*ANP32A (170−221) should be within 15 Å of the surface residues of 627 ($FluPol_E$ or $FluPol_R$) that are shifted upon interaction, and (b) residues from this region should lie within 40 Å of the RNA exit channel. This distance was chosen as representative of the distance between the midpoint of a 24 nucleotide RNA strand, and its two tethered ends (assumed immobilized on $FluPol_R$ and $FluPol_E$). A copy of NP was also placed in the RNA exit groove, with its RNA binding surface at 40 Å of the RNA exit channel and the sampling repeated, this time with the constraint that the binding region of *hu*ANP32A should lie within 15 Å of the RNA binding grooves, where ANP32A is also assumed to bind. For the *ch*ANP32A, the FluPol binding site should be within 15 Å of the surface residues of either 627 domain, and the NP binding site within 40 Å of the RNA exit channel. Different conformers that fulfill these restraints are shown in the figures to illustrate feasibility.

Cells. HEK-293T ANP32AB knockout (KO) cells were kindly provided by M Budt and T. Wolff (Robert Koch Institute, Berlin, Germany) and were grown in complete Dulbecco's modified Eagle's medium (DMEM, Gibco) supplemented with 10% fetal bovine serum (FBS) and 1% penicillin−streptomycin.

Plasmids for Cellular Assays. The A/WSN/33 (WSN, H1N1) pcDNA3.1-PB2, -PB1, -PA, and pCI-NP plasmids were described previously.[73,74] The pFluPol-HA-mCherry plasmid was generated by replacing the internal sequence of the pFluPol-HA plasmid of the WSN reverse genetic system[75] in between 125 nucleotides from the 5′ end and 77 nucleotides from the 3′ end by mCherry through standard PCR cloning followed by deletion of ATGs in the HA open-reading frame by an adapted site-directed mutagenesis protocol as described previously.[74] The coding sequence of huANP32 was generated by gene synthesis (GenScript Biotech) and cloned into the pCI vector by standard PCR cloning. The indicated mutations were introduced by site-directed mutagenesis.

vRNP Reconstitution Assay. The day before transfection, 3×10^4 HEK-293T ANP32AB KO cells were seeded in 96-well transparent plates (Corning 3599). The next day, cells were cotransfected using PEI (PEI MAX MW 40,000, Polysciences) with the following plasmids: 25 ng each of pcDNA3.1 PB2, PB1, PA, 50 ng of pCI-NP, 50 ng of pFluPol-HA-mCherry, and 50 ng of pCI-empty or huANP32A (WT or the indicated mutant). Fluorescence signals were acquired using the Incucyte S3 (Essen Bioscience) every 4 h (10× objective, 5 fields per well) and were analyzed using the Incucyte Live-Cell Analysis System (Sartorius) and are represented as RCU × μm^2/well.

■ ASSOCIATED CONTENT

Supporting Information

The Supporting Information is available free of charge at https://pubs.acs.org/doi/10.1021/jacs.3c06965.

Full presentation of the relaxation dispersion curves of NP titrated into solutions of *hu*ANP32A, cross correlated cross relaxation of different admixtures of 627(K)-NLS: *hu*ANP32A admixtures and ITC of human and avian ANP32A with NP (PDF)

■ AUTHOR INFORMATION

Corresponding Author

Martin Blackledge − *Institut de Biologie Structurale, Université Grenoble Alpes-CEA-CNRS UMR5075, 38000 Grenoble, France;* orcid.org/0000-0003-0935-721X; Email: martin.blackledge@ibs.fr

Authors

Aldo R. Camacho-Zarco − *Institut de Biologie Structurale, Université Grenoble Alpes-CEA-CNRS UMR5075, 38000 Grenoble, France;* orcid.org/0000-0002-0186-8544

Lefan Yu − *Institut de Biologie Structurale, Université Grenoble Alpes-CEA-CNRS UMR5075, 38000 Grenoble, France*

Tim Krischuns − *Institut Pasteur, Université Paris Cité, CNRS UMR3569, Unité Biologie des ARN et Virus Influenza, 75015 Paris, France*

Selin Dedeoglu − *Institut de Biologie Structurale, Université Grenoble Alpes-CEA-CNRS UMR5075, 38000 Grenoble, France;* Present Address: Centre de RMN à Très Hauts Champs, FRE 2034, University of Lyon, 69100 Villeurbanne, France

Damien Maurin − *Institut de Biologie Structurale, Université Grenoble Alpes-CEA-CNRS UMR5075, 38000 Grenoble, France*

Guillaume Bouvignies − *Laboratoire des Biomolécules, Département de Chimie, École Normale Supérieur, UPMC Université Paris 06, CNRS, PSL Research University, 75005 Paris, France;* orcid.org/0000-0003-4398-0320

Thibaut Crépin − *Institut de Biologie Structurale, Université Grenoble Alpes-CEA-CNRS UMR5075, 38000 Grenoble, France*

Rob W. H. Ruigrok − *Institut de Biologie Structurale, Université Grenoble Alpes-CEA-CNRS UMR5075, 38000 Grenoble, France*

Stephan Cusack − *European Molecular Biology Laboratory, 38000 Grenoble, France*

Nadia Naffakh − *Institut Pasteur, Université Paris Cité, CNRS UMR3569, Unité Biologie des ARN et Virus Influenza, 75015 Paris, France*

Complete contact information is available at: https://pubs.acs.org/10.1021/jacs.3c06965

Author Contributions

¶A.R.C.-Z. and L.Y. contributed equally to this work.

Funding

This work was supported by the European Research Council Advanced Grant Dynamic Assemblies under the European Union's Horizon 2020 research and innovation program (grant agreement number 835161) (M.B.). This work used the platforms of the Grenoble Instruct-ERIC center (ISBG; UAR 3518 CNRS-CEA-UGA-EMBL) within the Grenoble Partner-

ship for Structural Biology (PSB), supported by FRISBI (ANR-10-INBS-0005-02) and GRAL, financed within the University Grenoble Alpes graduate school (Ecoles Universitaires de Recherche) CBH-EUR-GS (ANR-17-EURE-0003). A.R.C.-Z. received funding from the European Union's Horizon 2020 research and innovation program under the Marie Skłodowska-Curie grant agreement no. 796490 and HFSP postdoctoral HFSP fellowship LT001544/2017. Financial support from the IR-RMN-THC Fr3050 CNRS for conducting the research is gratefully acknowledged. IBS acknowledges integration into the Interdisciplinary Research Institute of Grenoble (IRIG, CEA). We would like to thank M. Budt (Robert Koch Institute, Berlin, Germany) for providing HEK-293T ANP32AB knockout (KO) cells.

Notes

The authors declare no competing financial interest.

REFERENCES

(1) Nicholls, H. Pandemic Influenza: The Inside Story. *PLOS Biol.* **2006**, *4* (2), e50.
(2) Krammer, F.; Schultz-Cherry, S. We Need to Keep an Eye on Avian Influenza. *Nat. Rev. Immunol.* **2023**, *23* (5), 267−268.
(3) Wandzik, J. M.; Kouba, T.; Cusack, S. Structure and Function of Influenza Polymerase. *Cold Spring Harb. Perspect. Med.* **2021**, *11*, a038372.
(4) York, A.; Hengrung, N.; Vreede, F. T.; Huiskonen, J. T.; Fodor, E. Isolation and Characterization of the Positive-Sense Replicative Intermediate of a Negative-Strand RNA Virus. *Proc. Natl. Acad. Sci. U. S. A.* **2013**, *110* (45), E4238−4245.
(5) Fan, H.; Walker, A. P.; Carrique, L.; Keown, J. R.; Serna Martin, I.; Karia, D.; Sharps, J.; Hengrung, N.; Pardon, E.; Steyaert, J.; Grimes, J. M.; Fodor, E. Structures of Influenza A Virus RNA Polymerase Offer Insight into Viral Genome Replication. *Nature* **2019**, *573* (7773), 287−290.
(6) Chen, K.-Y.; Afonso, E. D. S.; Enouf, V.; Isel, C.; Naffakh, N. Influenza Virus Polymerase Subunits Co-Evolve to Ensure Proper Levels of Dimerization of the Heterotrimer. *PLOS Pathog.* **2019**, *15* (10), No. e1008034.
(7) Zhu, Z.; Fodor, E.; Keown, J. R. A Structural Understanding of Influenza Virus Genome Replication. *Trends Microbiol.* **2023**, *31* (3), 308−319.
(8) Tarendeau, F.; Boudet, J.; Guilligay, D.; Mas, P. J.; Bougault, C. M.; Boulo, S.; Baudin, F.; Ruigrok, R. W. H.; Daigle, N.; Ellenberg, J.; Cusack, S.; Simorre, J.-P.; Hart, D. J. Structure and Nuclear Import Function of the C-Terminal Domain of Influenza Virus Polymerase PB2 Subunit. *Nat. Struct. Mol. Biol.* **2007**, *14* (3), 229−233.
(9) Tarendeau, F.; Crepin, T.; Guilligay, D.; Ruigrok, R. W. H.; Cusack, S.; Hart, D. J. Host Determinant Residue Lysine 627 Lies on the Surface of a Discrete, Folded Domain of Influenza Virus Polymerase PB2 Subunit. *PLoS Pathog.* **2008**, *4* (8), No. e1000136.
(10) Kuzuhara, T.; Kise, D.; Yoshida, H.; Horita, T.; Murazaki, Y.; Nishimura, A.; Echigo, N.; Utsunomiya, H.; Tsuge, H. Structural Basis of the Influenza A Virus RNA Polymerase PB2 RNA-Binding Domain Containing the Pathogenicity-Determinant Lysine 627 Residue. *J. Biol. Chem.* **2009**, *284* (11), 6855−6860.
(11) Delaforge, E.; Milles, S.; Bouvignies, G.; Bouvier, D.; Boivin, S.; Salvi, N.; Maurin, D.; Martel, A.; Round, A.; Lemke, E. A.; Jensen, M. R.; Hart, D. J.; Blackledge, M. Large-Scale Conformational Dynamics Control H5N1 Influenza Polymerase PB2 Binding to Importin α. *J. Am. Chem. Soc.* **2015**, *137* (48), 15122−15134.
(12) Hengrung, N.; El Omari, K.; Serna Martin, I.; Vreede, F. T.; Cusack, S.; Rambo, R. P.; Vonrhein, C.; Bricogne, G.; Stuart, D. I.; Grimes, J. M.; Fodor, E. Crystal Structure of the RNA-Dependent RNA Polymerase from Influenza C Virus. *Nature* **2015**, *527* (7576), 114−117.
(13) Thierry, E.; Guilligay, D.; Kosinski, J.; Bock, T.; Gaudon, S.; Round, A.; Pflug, A.; Hengrung, N.; El Omari, K.; Baudin, F.; Hart, D. J.; Beck, M.; Cusack, S. Influenza Polymerase Can Adopt an Alternative Configuration Involving a Radical Repacking of PB2 Domains. *Mol. Cell* **2016**, *61* (1), 125−137.
(14) Subbarao, E. K.; Kawaoka, Y.; Murphy, B. R. Rescue of an Influenza A Virus Wild-Type PB2 Gene and a Mutant Derivative Bearing a Site-Specific Temperature-Sensitive and Attenuating Mutation. *J. Virol.* **1993**, *67* (12), 7223−7228.
(15) Massin, P.; van der Werf, S.; Naffakh, N. Residue 627 of PB2 Is a Determinant of Cold Sensitivity in RNA Replication of Avian Influenza Viruses. *J. Virol.* **2001**, *75* (11), 5398−5404.
(16) de Jong, M. D.; Simmons, C. P.; Thanh, T. T.; Hien, V. M.; Smith, G. J. D.; Chau, T. N. B.; Hoang, D. M.; Van Vinh Chau, N.; Khanh, T. H.; Dong, V. C.; Qui, P. T.; Van Cam, B.; Ha, D. Q.; Guan, Y.; Peiris, J. S. M.; Chinh, N. T.; Hien, T. T.; Farrar, J. Fatal Outcome of Human Influenza A (H5N1) Is Associated with High Viral Load and Hypercytokinemia. *Nat. Med.* **2006**, *12* (10), 1203−1207.
(17) Kirui, J.; Bucci, M. D.; Poole, D. S.; Mehle, A. Conserved Features of the PB2 627 Domain Impact Influenza Virus Polymerase Function and Replication. *J. Virol.* **2014**, *88* (11), 5977−5986.
(18) Huyton, T.; Wolberger, C. The Crystal Structure of the Tumor Suppressor Protein Pp32 (Anp32a): Structural Insights into Anp32 Family of Proteins. *Protein Sci. Publ. Protein Soc.* **2007**, *16* (7), 1308−1315.
(19) de Chiara, C.; Menon, R. P.; Pastore, A. Structural Bases for Recognition of Anp32/LANP Proteins. *FEBS J.* **2008**, *275* (10), 2548−2560.
(20) Long, J. S.; Giotis, E. S.; Moncorgé, O.; Frise, R.; Mistry, B.; James, J.; Morisson, M.; Iqbal, M.; Vignal, A.; Skinner, M. A.; Barclay, W. S. Species Difference in ANP32A Underlies Influenza A Virus Polymerase Host Restriction. *Nature* **2016**, *529* (7584), 101−104.
(21) Sugiyama, K.; Kawaguchi, A.; Okuwaki, M.; Nagata, K. Pp32 and APRIL Are Host Cell-Derived Regulators of Influenza Virus RNA Synthesis from CRNA. *eLife* **2015**, *4*, No. e08939.
(22) Lowen, A. C. Virology: Host Protein Clips Bird Flu's Wings in Mammals. *Nature* **2016**, *529* (7584), 30−31.
(23) Mehle, A. The Avian Influenza Virus Polymerase Brings ANP32A Home to Roost. *Cell Host Microbe* **2016**, *19* (2), 137−138.
(24) Domingues, P.; Hale, B. G. Functional Insights into ANP32A-Dependent Influenza A Virus Polymerase Host Restriction. *Cell Rep.* **2017**, *20* (11), 2538−2546.
(25) Baker, S. F.; Ledwith, M. P.; Mehle, A. Differential Splicing of ANP32A in Birds Alters Its Ability to Stimulate RNA Synthesis by Restricted Influenza Polymerase. *Cell Rep.* **2018**, *24* (10), 2581−2588.e4.
(26) Long, J. S.; Mistry, B.; Haslam, S. M.; Barclay, W. S. Host and Viral Determinants of Influenza A Virus Species Specificity. *Nat. Rev. Microbiol.* **2019**, *17* (2), 67.
(27) Staller, E.; Sheppard, C. M.; Neasham, P. J.; Mistry, B.; Peacock, T. P.; Goldhill, D. H.; Long, J. S.; Barclay, W. S. ANP32 Proteins Are Essential for Influenza Virus Replication in Human Cells. *J. Virol.* **2019**, *93* (17), e00217−19.
(28) Zhang, H.; Zhang, Z.; Wang, Y.; Wang, M.; Wang, X.; Zhang, X.; Ji, S.; Du, C.; Chen, H.; Wang, X. Fundamental Contribution and Host Range Determination of ANP32A and ANP32B in Influenza A Virus Polymerase Activity. *J. Virol.* **2019**, *93* (13). DOI: 10.1128/JVI.00174-19.
(29) Baker, S. F.; Mehle, A. ANP32B, or Not to Be, That Is the Question for Influenza Virus. *eLife* **2019**, *8*, No. e48084.
(30) Long, J. S.; Idoko-Akoh, A.; Mistry, B.; Goldhill, D.; Staller, E.; Schreyer, J.; Ross, C.; Goodbourn, S.; Shelton, H.; Skinner, M. A.; Sang, H.; McGrew, M. J.; Barclay, W. Species Specific Differences in Use of ANP32 Proteins by Influenza A Virus. *eLife* **2019**, *8*, No. e45066.
(31) Mistry, B.; Long, J. S.; Schreyer, J.; Staller, E.; Sanchez-David, R. Y.; Barclay, W. S. Elucidating the Interactions between Influenza Virus Polymerase and Host Factor ANP32A. *J. Virol.* **2020**, *94* (3). DOI: 10.1128/JVI.01353-19.
(32) Camacho-Zarco, A. R.; Kalayil, S.; Maurin, D.; Salvi, N.; Delaforge, E.; Milles, S.; Jensen, M. R.; Hart, D. J.; Cusack, S.;

Blackledge, M. Molecular Basis of Host-Adaptation Interactions between Influenza Virus Polymerase PB2 Subunit and ANP32A. *Nat. Commun.* **2020**, *11* (1), 3656.
(33) Camacho-Zarco, A. R.; Schnapka, V.; Guseva, S.; Abyzov, A.; Adamski, W.; Milles, S.; Jensen, M. R.; Zidek, L.; Salvi, N.; Blackledge, M. NMR Provides Unique Insight into the Functional Dynamics and Interactions of Intrinsically Disordered Proteins. *Chem. Rev.* **2022**, *122*, 9331−9356.
(34) Fodor, E.; Te Velthuis, A. J. W. Structure and Function of the Influenza Virus Transcription and Replication Machinery. *Cold Spring Harb. Perspect. Med.* **2020**, *10*, No. a038398.
(35) Peacock, T. P.; Sheppard, C. M.; Staller, E.; Barclay, W. S. Host Determinants of Influenza RNA Synthesis. *Annu. Rev. Virol.* **2019**, *6* (1), 215−233.
(36) Swann, O. C.; Rasmussen, A. B.; Peacock, T. P.; Sheppard, C. M.; Barclay, W. S. Avian Influenza A Virus Polymerase Can Utilize Human ANP32 Proteins To Support CRNA but Not VRNA Synthesis. *mBio* **2023**, *14* (1), e03399−22.
(37) Carrique, L.; Fan, H.; Walker, A. P.; Keown, J. R.; Sharps, J.; Staller, E.; Barclay, W. S.; Fodor, E.; Grimes, J. M. Host ANP32A Mediates the Assembly of the Influenza Virus Replicase. *Nature* **2020**, *587* (7835), 638−643.
(38) Masters, P. S.; Banerjee, A. K. Complex Formation with Vesicular Stomatitis Virus Phosphoprotein NS Prevents Binding of Nucleocapsid Protein N to Nonspecific RNA. *J. Virol.* **1988**, *62* (8), 2658−2664.
(39) Curran, J.; Marq, J.; Kolakofsky, D. An N-Terminal Domain of the Sendai Paramyxovirus P-Protein Acts as a Chaperone for the Np Protein During the Nascent Chain Assembly Step of Genome Replication. *J. Virol.* **1995**, *69* (2), 849−855.
(40) Leyrat, C.; Yabukarski, F.; Tarbouriech, N.; Ribeiro, E. A.; Jensen, M. R.; Blackledge, M.; Ruigrok, R. W. H.; Jamin, M. Structure of the Vesicular Stomatitis Virus N^0-P Complex. *PLoS Pathog.* **2011**, *7* (9), No. e1002248.
(41) Guseva, S.; Milles, S.; Blackledge, M.; Ruigrok, R. W. H. The Nucleoprotein and Phosphoprotein of Measles Virus. *Front. Microbiol.* **2019**, *10*, 1832.
(42) Hoenen, T.; Shabman, R. S.; Groseth, A.; Herwig, A.; Weber, M.; Schudt, G.; Dolnik, O.; Basler, C. F.; Becker, S.; Feldmann, H. Inclusion Bodies Are a Site of Ebolavirus Replication. *J. Virol.* **2012**, *86* (21), 11779−11788.
(43) Nikolic, J.; Le Bars, R.; Lama, Z.; Scrima, N.; Lagaudrière-Gesbert, C.; Gaudin, Y.; Blondel, D. Negri Bodies Are Viral Factories with Properties of Liquid Organelles. *Nat. Commun.* **2017**, *8* (1), 58.
(44) Heinrich, B. S.; Maliga, Z.; Stein, D. A.; Hyman, A. A.; Whelan, S. P. J. Phase Transitions Drive the Formation of Vesicular Stomatitis Virus Replication Compartments. *mBio* **2018**, *9* (5). DOI: 10.1128/mBio.02290-17.
(45) Ma, D.; George, C. X.; Nomburg, J. L.; Pfaller, C. K.; Cattaneo, R.; Samuel, C. E. Upon Infection, Cellular WD Repeat-Containing Protein 5 (WDR5) Localizes to Cytoplasmic Inclusion Bodies and Enhances Measles Virus Replication. *J. Virol.* **2018**, *92* (5), e01726−17.
(46) Guseva, S.; Milles, S.; Jensen, M. R.; Salvi, N.; Kleman, J.-P.; Maurin, D.; Ruigrok, R. W. H.; Blackledge, M. Measles Virus Nucleo- and Phosphoproteins Form Liquid-like Phase-Separated Compartments That Promote Nucleocapsid Assembly. *Sci. Adv.* **2020**, *6* (14), No. eaaz7095.
(47) Wang, F.; Sheppard, C. M.; Mistry, B.; Staller, E.; Barclay, W. S.; Grimes, J. M.; Fodor, E.; Fan, H. The C-Terminal LCAR of Host ANP32 Proteins Interacts with the Influenza A Virus Nucleoprotein to Promote the Replication of the Viral RNA Genome. *Nucleic Acids Res.* **2022**, *50* (10), 5713−5725.
(48) Chenavas, S.; Estrozi, L. F.; Slama-Schwok, A.; Delmas, B.; Di Primo, C.; Baudin, F.; Li, X.; Crépin, T.; Ruigrok, R. W. H. Monomeric Nucleoprotein of Influenza A Virus. *PLoS Pathog.* **2013**, *9* (3), No. e1003275.
(49) Tang, Y.-S.; Xu, S.; Chen, Y.-W.; Wang, J.-H.; Shaw, P.-C. Crystal Structures of Influenza Nucleoprotein Complexed with Nucleic Acid Provide Insights into the Mechanism of RNA Interaction. *Nucleic Acids Res.* **2021**, *49* (7), 4144−4154.
(50) Bernado, P.; Blanchard, L.; Timmins, P.; Marion, D.; Ruigrok, R. W. H.; Blackledge, M. A Structural Model for Unfolded Proteins from Residual Dipolar Couplings and Small-Angle x-Ray Scattering. *Proc. Natl. Acad. Sci. U. S. A.* **2005**, *102* (47), 17002−17007.
(51) Ozenne, V.; Bauer, F.; Salmon, L.; Huang, J.-R.; Jensen, M. R.; Segard, S.; Bernadó, P.; Charavay, C.; Blackledge, M. Flexible-Meccano: A Tool for the Generation of Explicit Ensemble Descriptions of Intrinsically Disordered Proteins and Their Associated Experimental Observables. *Bioinforma. Oxf. Engl.* **2012**, *28* (11), 1463−1470.
(52) Curran, J.; Kolakofsky, D. Replication of Paramyxoviruses. *Adv. Virus Res.* **1999**, *54*, 403−422.
(53) Yabukarski, F.; Lawrence, P.; Tarbouriech, N.; Bourhis, J.-M.; Delaforge, E.; Jensen, M. R.; Ruigrok, R. W. H.; Blackledge, M.; Volchkov, V.; Jamin, M. Structure of Nipah Virus Unassembled Nucleoprotein in Complex with Its Viral Chaperone. *Nat. Struct. Mol. Biol.* **2014**, *21* (9), 754−759.
(54) Milles, S.; Jensen, M. R.; Lazert, C.; Guseva, S.; Ivashchenko, S.; Communie, G.; Maurin, D.; Gerlier, D.; Ruigrok, R. W. H.; Blackledge, M. An Ultraweak Interaction in the Intrinsically Disordered Replication Machinery Is Essential for Measles Virus Function. *Sci. Adv.* **2018**, *4* (8), No. eaat7778.
(55) Guseva, S.; Milles, S.; Jensen, M. R.; Schoehn, G.; Ruigrok, R. W.; Blackledge, M. Structure, Dynamics and Phase Separation of Measles Virus RNA Replication Machinery. *Curr. Opin. Virol.* **2020**, *41*, 59−67.
(56) Mittag, T.; Orlicky, S.; Choy, W.-Y.; Tang, X.; Lin, H.; Sicheri, F.; Kay, L. E.; Tyers, M.; Forman-Kay, J. D. Dynamic Equilibrium Engagement of a Polyvalent Ligand with a Single-Site Receptor. *Proc. Natl. Acad. Sci. U. S. A.* **2008**, *105* (46), 17772−17777.
(57) Li, P.; Banjade, S.; Cheng, H.-C.; Kim, S.; Chen, B.; Guo, L.; Llaguno, M.; Hollingsworth, J. V.; King, D. S.; Banani, S. F.; Russo, P. S.; Jiang, Q.-X.; Nixon, B. T.; Rosen, M. K. Phase Transitions in the Assembly of Multivalent Signalling Proteins. *Nature* **2012**, *483* (7389), 336−340.
(58) Fung, H. Y. J.; Birol, M.; Rhoades, E. IDPs in Macromolecular Complexes: The Roles of Multivalent Interactions in Diverse Assemblies. *Curr. Opin. Struct. Biol.* **2018**, *49*, 36−43.
(59) Borgia, A.; Borgia, M. B.; Bugge, K.; Kissling, V. M.; Heidarsson, P. O.; Fernandes, C. B.; Sottini, A.; Soranno, A.; Buholzer, K. J.; Nettels, D.; Kragelund, B. B.; Best, R. B.; Schuler, B. Extreme Disorder in an Ultrahigh-Affinity Protein Complex. *Nature* **2018**, *555* (7694), 61−66.
(60) Sottini, A.; Borgia, A.; Borgia, M. B.; Bugge, K.; Nettels, D.; Chowdhury, A.; Heidarsson, P. O.; Zosel, F.; Best, R. B.; Kragelund, B. B.; Schuler, B. Polyelectrolyte Interactions Enable Rapid Association and Dissociation in High-Affinity Disordered Protein Complexes. *Nat. Commun.* **2020**, *11* (1), 5736.
(61) Milles, S.; Mercadante, D.; Aramburu, I. V.; Jensen, M. R.; Banterle, N.; Koehler, C.; Tyagi, S.; Clarke, J.; Shammas, S. L.; Blackledge, M.; Graeter, F.; Lemke, E. A. Plasticity of an Ultrafast Interaction between Nucleoporins and Nuclear Transport Receptors. *Cell* **2015**, *163* (3), 734−745.
(62) Pak, C. W.; Kosno, M.; Holehouse, A. S.; Padrick, S. B.; Mittal, A.; Ali, R.; Yunus, A. A.; Liu, D. R.; Pappu, R. V.; Rosen, M. K. Sequence Determinants of Intracellular Phase Separation by Complex Coacervation of a Disordered Protein. *Mol. Cell* **2016**, *63* (1), 72−85.
(63) Pflug, A.; Guilligay, D.; Reich, S.; Cusack, S. Structure of Influenza A Polymerase Bound to the Viral RNA Promoter. *Nature* **2014**, *516* (7531), 355−360.
(64) Peng, Q.; Liu, Y.; Peng, R.; Wang, M.; Yang, W.; Song, H.; Chen, Y.; Liu, S.; Han, M.; Zhang, X.; Wang, P.; Yan, J.; Zhang, B.; Qi, J.; Deng, T.; Gao, G. F.; Shi, Y. Structural Insight into RNA Synthesis by Influenza D Polymerase. *Nat. Microbiol.* **2019**, *4* (10), 1750−1759.

(65) Kouba, T.; Drncová, P.; Cusack, S. Structural Snapshots of Actively Transcribing Influenza Polymerase. *Nat. Struct. Mol. Biol.* **2019**, *26* (6), 460−470.
(66) Delaglio, F.; Grzesiek, S.; Vuister, G.; Zhu, G.; Pfeifer, J.; Bax, A. Nmrpipe - A Multidimensional Spectral Processing System Based On Unix Pipes. *J. Biomol. NMR* **1995**, *6* (3), 277−293.
(67) Lee, W.; Tonelli, M.; Markley, J. L. NMRFAM-SPARKY: Enhanced Software for Biomolecular NMR Spectroscopy. *Bioinforma. Oxf. Engl.* **2015**, *31* (8), 1325−1327.
(68) Lakomek, N.-A.; Ying, J.; Bax, A. Measurement of ^{15}N Relaxation Rates in Perdeuterated Proteins by TROSY-Based Methods. *J. Biomol. NMR* **2012**, *53* (3), 209−221.
(69) Pelupessy, P.; Espallargas, G. M.; Bodenhausen, G. Symmetrical Reconversion: Measuring Cross-Correlation Rates with Enhanced Accuracy. *J. Magn. Reson. San Diego Calif 1997* **2003**, *161* (2), 258−264.
(70) Meiboom, S.; Gill, D. Modified Spin-Echo Method for Measuring Nuclear Relaxation Times. *Rev. Sci. Instrum.* **1958**, *29* (8), 688−691.
(71) Carr, H. Y.; Purcell, E. M. Effects of Diffusion on Free Precession in Nuclear Magnetic Resonance Experiments. *Phys. Rev.* **1954**, *94* (3), 630−638.
(72) Hansen, D. F.; Vallurupalli, P.; Kay, L. E. An Improved 15N Relaxation Dispersion Experiment for the Measurement of Millisecond Time-Scale Dynamics in Proteins. *J. Phys. Chem. B* **2008**, *112* (19), 5898−5904.
(73) Lukarska, M.; Fournier, G.; Pflug, A.; Resa-Infante, P.; Reich, S.; Naffakh, N.; Cusack, S. Structural Basis of an Essential Interaction between Influenza Polymerase and Pol II CTD. *Nature* **2017**, *541* (7635), 117−121.
(74) Krischuns, T.; Isel, C.; Drncova, P.; Lukarska, M.; Pflug, A.; Paisant, S.; Navratil, V.; Cusack, S.; Naffakh, N. Type B and Type A Influenza Polymerases Have Evolved Distinct Binding Interfaces to Recruit the RNA Polymerase II CTD. *PLoS Pathog.* **2022**, *18* (5), No. e1010328.
(75) Fodor, E.; Devenish, L.; Engelhardt, O. G.; Palese, P.; Brownlee, G. G.; García-Sastre, A. Rescue of Influenza A Virus from Recombinant DNA. *J. Virol.* **1999**, *73* (11), 9679−9682.

https://doi.org/10.1021/jacs.3c06965
J. Am. Chem. Soc. 2023, 145, 20985−21001